Measurement of Correlation Between Flow Density, Velocity, and Density*Velocity^2 With Far Field Noise in High Speed Jets

Jayanta Panda
Ohio Aerospace Institute, Brook Park, Ohio

Richard G. Seasholtz
Glenn Research Center, Cleveland, Ohio

Kristie A. Elam
Akima Corporation, Fairview Park, Ohio

September 2002

The NASA STI Program Office . . . in Profile

Since its founding, NASA has been dedicated to the advancement of aeronautics and space science. The NASA Scientific and Technical Information (STI) Program Office plays a key part in helping NASA maintain this important role.

The NASA STI Program Office is operated by Langley Research Center, the Lead Center for NASA's scientific and technical information. The NASA STI Program Office provides access to the NASA STI Database, the largest collection of aeronautical and space science STI in the world. The Program Office is also NASA's institutional mechanism for disseminating the results of its research and development activities. These results are published by NASA in the NASA STI Report Series, which includes the following report types:

- TECHNICAL PUBLICATION. Reports of completed research or a major significant phase of research that present the results of NASA programs and include extensive data or theoretical analysis. Includes compilations of significant scientific and technical data and information deemed to be of continuing reference value. NASA's counterpart of peer-reviewed formal professional papers but has less stringent limitations on manuscript length and extent of graphic presentations.

- TECHNICAL MEMORANDUM. Scientific and technical findings that are preliminary or of specialized interest, e.g., quick release reports, working papers, and bibliographies that contain minimal annotation. Does not contain extensive analysis.

- CONTRACTOR REPORT. Scientific and technical findings by NASA-sponsored contractors and grantees.

- CONFERENCE PUBLICATION. Collected papers from scientific and technical conferences, symposia, seminars, or other meetings sponsored or cosponsored by NASA.

- SPECIAL PUBLICATION. Scientific, technical, or historical information from NASA programs, projects, and missions, often concerned with subjects having substantial public interest.

- TECHNICAL TRANSLATION. English-language translations of foreign scientific and technical material pertinent to NASA's mission.

Specialized services that complement the STI Program Office's diverse offerings include creating custom thesauri, building customized databases, organizing and publishing research results . . . even providing videos.

For more information about the NASA STI Program Office, see the following:

- Access the NASA STI Program Home Page at *http://www.sti.nasa.gov*

- E-mail your question via the Internet to help@sti.nasa.gov

- Fax your question to the NASA Access Help Desk at 301–621–0134

- Telephone the NASA Access Help Desk at 301–621–0390

- Write to:
  NASA Access Help Desk
  NASA Center for AeroSpace Information
  7121 Standard Drive
  Hanover, MD 21076

Measurement of Correlation Between Flow Density, Velocity, and Density*Velocity^2 With Far Field Noise in High Speed Jets

Jayanta Panda
Ohio Aerospace Institute, Brook Park, Ohio

Richard G. Seasholtz
Glenn Research Center, Cleveland, Ohio

Kristie A. Elam
Akima Corporation, Fairview Park, Ohio

National Aeronautics and
Space Administration

Glenn Research Center

September 2002

Acknowledgments

This report is a formal draft or working
paper, intended to solicit comments and
ideas from a technical peer group.

Measurement of Correlation Between Flow Density, Velocity, and Density*Velocity[2] With Far Field Noise in High Speed Jets

Jayanta Panda
Ohio Aerospace Institute
Brook Park, Ohio 44142

Richard G. Seasholtz
National Aeronautics and Space Administration
Glenn Research Center
Cleveland, Ohio 44135

Kristie A. Elam
Akima Corporation
Fairview Park, Ohio 44126

Abstract

To locate noise sources in high-speed jets, the sound pressure fluctuations p', measured at far field locations, were correlated with each of radial velocity v, density ρ, and ρv^2 fluctuations measured from various points in jet plumes. The experiments follow the cause-and-effect method of sound source identification, where $<\rho v^2\text{-}p'>$ correlation is related to the first, and $<\rho\text{-}p'>$ correlation to the second source terms of Lighthill's equation. Three fully expanded, unheated plumes of Mach number 0.95, 1.4 and 1.8 were studied for this purpose. The velocity and density fluctuations were measured simultaneously using a recently developed, non-intrusive, point measurement technique based on molecular Rayleigh scattering (Seasholtz, Panda & Elam, *AIAA paper no 2002-0827*). The technique uses a continuous wave, narrow line-width laser, Fabry-Perot interferometer and photon counting electronics. Light scattered by air molecules from a point on the laser beam was collected and spectrally resolved by a Fabry-Perot Interferometer. The Doppler shift from the incident laser frequency was measured by splitting the image, formed after the interferometer, into two parts and measuring the intensity-ratio by a pair of photomultiplier tubes. This ultimately provided a time history of velocity variations v(t). A part of the Rayleigh scattered light was measured directly, without passing through the interferometer, using a third photo-multiplier tube to obtain a time history of density fluctuations ρ(t); and finally, multiplications of the time series data provided ρv^2(t). Fourier transforms of the time series data provided respective spectra. It was observed that along the jet centerline the density fluctuation spectra S_ρ have different shapes than the radial velocity spectra S_v, while data obtained from the peripheral shear layer show similarity between the two spectra. To determine sources of sound pressure fluctuations, at 30° and 90° to the jet axis, microphone signals from 50 nozzle diameters and these two azimuthal locations were cross-correlated with individual flow variables. Density fluctuations in the jet showed significantly higher correlation, than either ρv^2 or v fluctuations, with either of the microphone signals. It is found that a single point $<\rho\text{-}p'>$ correlation from the peak sound emitting region at the end of the potential core can account for nearly 10% of all noise at 30° to the jet axis. The $<\rho v^2\text{-}p'>$ correlation, representing the effectiveness of a longitudinal quadrupole in generating noise 90° to the jet axis, is found to be zero within experimental uncertainty. In contrast ρv^2 fluctuations were better correlated with sound pressure fluctuation at the 30° location. Some other interesting observations are following. In general, correlation from the 90° microphone is significantly poorer than that from the 30° microphone. The strongest source of sound at either microphone stations is found to lie at the centerline and beyond the end of potential core.

I. INTRODUCTION

Last six decades of research has not produced a unanimously accepted answer to the simple question of what produces noise from a jet flow. A vast number of earlier and current researchers have relied upon the acoustic analogy framework of Lighthill (1952), Lilley (1972) and others. The Lighthill's equation is:

$$\frac{\partial^2 \rho'}{\partial t^2} - a_0^2 \nabla^2 \rho' = \frac{\partial^2 T_{ij}}{\partial X_i \, \partial X_j};$$

(1)

$$T_{ij} = \rho U_i\, U_j + \delta_{ij}(p' - a_0^2 \rho')$$

Where ρ is air density, ρ' fluctuating density, p' fluctuating pressure, a_0 ambient speed of sound, and U_i velocity vector and T_{ij} are the stress tensors. In the last few years there has been a steady growth of opposition to such an answer, based on multiple issues (Fedorchenko 2000, Tam 2001). A critical factor that has

fueled the controversy is a lack of experimental verification of Lighthill sources, besides the U^8 dependence of sound intensity, which only confirms proper dimensional scaling. One aspect of the controversy is very apparent: Lighthill's equation is nothing but a reformulation of the mass and momentum conservation equations and therefore, every solution upholds these two physical laws. It is known that only a small part of the disturbances created by turbulent motion inside a jet ultimately radiates as sound. Since both radiating and non-radiating disturbances satisfy the same conservation laws, Lighthill's equation is unable to separate the two.

Additional criteria are necessary, such as a frequency-wave number, ω-κ, analysis of the turbulent motion and imposition of a condition of supersonic convective speed with respect to the ambient: $\omega/\kappa \geq a_0$. This additional criterion has been discussed by Goldstein (1976), practiced regularly to calculate the far field sound from instability waves (Morris & Tam 1979, Tam & Burton 1984), and recently applied by Freund (2001) to calculate sound sources from the Direct Numerical Simulation of a low Reynolds number jet. Freund calculated the Lighthill stress tensor and then applied the above constrain to extract sound sources. All of these computational and analytical efforts have made the need for an independent verification of sound sources even greater. Experimentally, thus far it has been impossible to directly measure the stress tensors. The common practice of using microphone arrays, elliptic and spherical mirrors in the far field to determine source location has both advantages and serious drawbacks. By placing a listening device in the far field the separation problem between radiating and non-radiating disturbances is naturally avoided as the pressure fluctuations that arrive far away from the turbulent plume are by definition radiated waves. On the other hand, sound waves undergo a large amount of refraction and scattering before arriving at the far field; a linear extrapolation of sound path may lead to a wrong conclusion. In addition, such methods depend on a monopole model of noise source distribution, which is as good as the subjective expectation used for the modeling. There is a need to validate any model or acoustic analogy via independent means, which is the motivation for the present work. It can be argued that such an independent means can neither be achieved by only turbulence measurement/ simulation, nor by sole observations from far field, but through a simultaneous measurement of turbulent fluctuations (cause) and the far noise field (effect).

The direct correlation between the cause and effect was originally proposed by Siddon (see Siddon 1973, Rackl 1972) to locate sound sources, and during the 1970's many experimentalists had taken on the method.

Usually, velocity (Lee & Ribner 1972, Seiner & Reethof 1974, Schaffer 1979, Richarz 1979 and others) or pressure fluctuations (Hurdle, Meecham & Hodder 1974, Armstrong et al 1977 and others) in the jet were correlated with the sound pressure fluctuation measured by a fixed microphone. One attractive feature of this method is that the effects of scattering, absorption and refraction on sound radiation are automatically included by virtue of simultaneously extracting information from both the flow and acoustic fields. Another advantage in calculating the Lighthill source strength is that the fourth order derivative of the stress tensor is reduced to a second order one. Unfortunately, the promises were mostly unfulfilled in the earlier work primarily due to a lack of unobtrusive turbulence measurement technique. The noise produced by intrusive hot-wire probes (Seiner 1974, and others) or microphones (Hurdle, Meecham & Hodder, 1974 and others) placed inside the flow contributed to most of the correlation. Later on Laser Doppler Velocimetry (LDV) was used by Schaffer (1979) and Richarz (1979) among others. Schaffer wrote down the vast number of approximations and assumptions needed to relate the experimental data to theory. Nevertheless, the important issue of accuracy in velocity spectra measurements using LDV has lingered. The issues of seed particles following turbulent eddies, various biasing errors, and the high level of noise makes LDV a difficult tool to measure turbulence spectrum. An approximation, used by earlier researchers in evaluating Lighthill's stress tensors, is that the contribution from the density fluctuation is negligible: $\rho U_i U_j \approx \overline{\rho} U_i U_j$, where $\overline{\rho}$ is time averaged density. The present experiment, on the other hand, shows that density fluctuations have the highest correlation with far-field noise. It is to be noted that the role of density in Lighthill's formulation is ambivalent, every term in cause (right hand side of equation 1) and in effect (left hand side) contains a dependence on density.

Recently, a molecular Rayleigh scattering based technique has been advanced to simultaneously measure density and velocity fluctuations spectra in high-speed flow for the first time (Seasholtz, Panda & Elam, 2001, 2002). Fluctuations occurring over a large frequency range: up to 25KHz, have been measured. The technique is based on laser light scattering from the gas molecules present in air. Since neither any seed particles nor any intrusive probes are used the technique is free from various problems faced by previous researchers. Air density fluctuation is the easiest to measure and has the highest accuracy. An in depth study of correlation between flow density fluctuations and sound pressure fluctuations from the peak noise emission direction had been reported earlier (panda & Seasholtz, 2002). The present work is a continuation and banks on the additional capability of measuring one component of velocity fluctuations.

Causality relation: Following is a recollection of the principles behind the Causality relation. The free space solution for the Lighthill's wave equation for a field point $\mathbf{X_f}$ from distributed source points $\mathbf{X_s}$ (Fig. 1) is:

$$p'(\mathbf{X_f};t) = \frac{1}{4\pi}\frac{\partial^2}{\partial X_i \partial X_j}\int_V T_{ij}(\mathbf{X_s};t')\frac{d^3\mathbf{X_s}}{|\mathbf{X_f}-\mathbf{X_s}|} \quad (2)$$

Where, p' represents pressure fluctuations and the terms inside the integral are calculated at a retarded time to account for propagation from the source point to the field point: $t' = t - \tau_0$, $\tau_0 = |\mathbf{X_f}-\mathbf{X_s}|/a_0$. The integral is taken over the whole jet volume $\mathbf{V}$. Equation 1 shows that the stress tensor T_{ij} has two terms. The first term $\frac{\partial^2(\rho U_i U_j)}{\partial X_i \partial X_j}$ has 9 different components, out of which the contribution from ρvv (v is radial component of velocity) fluctuations is measured in the present work. In the following, at first, the traditional approach of applying the causality relationship to the ρvv term is outlined. Various issues involved in the interpretation are discussed next. Finally an extension of the causality relation to include the second term that depends on the thermodynamic quantities is outlined.

Following Proudman's analysis (1952), the double space divergence can be converted into double time derivative under two restrictions: (a) a scalar component of the stress tensor is measured along the direction of observation from the source, and (b) the field point is far enough to be in the radiation field of all sources. Under these conditions, the acoustic pressure at the field point can be written as:

$$p'(\mathbf{X_f};t) = \frac{1}{4\pi a_0^2 \mathbf{r}}\int_V \frac{\partial^2}{\partial t'^2}\left[\rho v^2(\mathbf{X_s};t')\right]d^3\mathbf{X_s} \quad (3)$$

where $\mathbf{r}$ is radial distance. The scalar component of the stress tensor of interest represents a longitudinal quadrupole, made by on axis positioning of two opposite dipoles. Such a quadrupole has very strong directivity and, in the absence of convective amplification, the acoustic intensity falls as the $\cos^4$ from the peak radiation direction. Since v represents the measured radial component of velocity the peak radiation direction is along 90° to the jet axis. Notably along this direction acoustic intensity is unaffected by convective amplification.

To obtain acoustic intensity an autocorrelation function for the above equation needs to be worked out. Usually, the auto-correlation function is created by multiplying space-time separated stress tensors:

$$\left\langle p'^2 \right\rangle(\mathbf{X_f};t) = \quad (4)$$

$$\frac{1}{16\pi^2 a_0^4 \mathbf{r}^2}\int_V \frac{\partial^4}{\partial t^4}\left\langle \rho v^2(\mathbf{X_s};t')\rho v^2(\mathbf{X_s}+\Delta\mathbf{X};t'+\Delta t')\right\rangle d^3\mathbf{X_s}$$

In the "causality" relationship, however; this is accomplished by multiplying the source integral with the far field sound pressure:

$$\left\langle p'^2 \right\rangle(\mathbf{X_f};\tau) =$$

$$\left\langle \left[\frac{1}{4\pi a_0^2 \mathbf{r}}\int_V \frac{\partial^2}{\partial t'^2}\left[\rho v^2(\mathbf{X_s};t')\right]d^3\mathbf{X_s}\right]\left[p'(\mathbf{X_f};t)\right]\right\rangle$$

$$= \frac{1}{4\pi \mathbf{r} a_0^2}\int_V \frac{\partial^2}{\partial \tau^2}\left[R_{\rho vv;p'}(\mathbf{X_s},\mathbf{X_f};\tau)\right]d^3\mathbf{X_s} \quad (5)$$

where, $R_{\rho vv;p'}(\mathbf{X_s},\mathbf{X_f};\tau) =$

$$\left\langle \rho v^2(\mathbf{X_s};t+\tau-\tau_0)\, p'(\mathbf{X_f};t)\right\rangle$$

The $< >$ bracketed expressions imply a time average. Also, the correlation function $R_{\rho vv;p'}$ has to be calculated after shifting the ρv^2 data by the propagation time $\tau = -\tau_0$, or inversely the pressure fluctuation data by $\tau = \tau_0$. In essence, equation 5 expresses the radiated acoustic field in terms of an integral taken over the entire source volume, and consists of correlation functions between far field sound pressure and source field ρv^2. It is interesting to point out a particular advantage of equation 5 over 4. It has been discussed earlier that the Lighthill's' equation is unable to separate the propagating and non-propagating parts of the disturbances. The traditional auto-correlation function in equation 4 is created by correlating two source points. In order to determine which part of this correlation ultimately radiates as sound, an additional wave number – frequency analysis of the right hand side is required (Morris et al 2002, Goldstein, 1976). On the other hand, the field point to source point correlation, employed in the causality method is free from the additional complication; since by definition a microphone kept in a far-field location only senses the radiated part of disturbances.

In the present paper, data analysis is performed in narrowband frequencies. Fourier transform of equation 5 yields (noting that the autocorrelation function is transformed to power spectral density and cross-correlation to cross-spectrum, and the real part of the cross-spectrum function has to be used):

$$S_{p'^2}(\mathbf{X_f};f)\,df =$$

$$-\frac{\pi f^2\,df}{\mathbf{r} a_0^2}\,\mathrm{Re}\left\{\int_V S_{\rho vv,p'}(\mathbf{X_f},\mathbf{X_s};f)\,d^3\mathbf{X_s}\right\} \quad (6)$$

cross$-$spectrum: $S_{\rho vv,p'}(\mathbf{X_f},\mathbf{X_s};f) =$

$$\int_{-\infty}^{\infty} R_{\rho vv;p'}(\mathbf{X_s},\mathbf{X_f};\tau)\exp(-j2\pi f\tau)\,d\tau$$

Here Re represents real part. Finally, the acoustic intensity at the field point $\mathbf{X_f}$:

$$I(\mathbf{X_f}) = \frac{1}{a_0 \rho_0} \int_{-\infty}^{\infty} S_{p'2} \, df =$$

$$-\frac{\pi}{r\rho_0 a_0^3} \, Re \left\{ \int_{-\infty}^{\infty} \int_V f^2 S_{\rho vv, p'}(X_f, X_s; f) d^3 X_s \, df \right\} \quad (7)$$

The above equation shows that the intensity of sound radiation is directly dependent on the distribution of cross-spectrum function in the flow field.

There are multiple issues surrounding the causality method. At a first glance the right hand sides of equations 4 & 5 are expected to be equal although the integrands are different. However, they may not be so as the difference between propagating and non-propagating disturbances is included in the latter. There is an issue of non-uniqueness in the application of causality method (Ffowcs Williams 1973). Since the sound pressure at the field point is a large sum over the entire sound-producing region of the jet, an unlimited number of variations in the source correlation can lead to the same summation at the field point. This criticism is not special for the causality technique but in general true for the more common form of source description via two-source points correlation (eqn. 4), which likewise, has to be integrated over the source volume. In a broader sense, many inverse problems in physics are of this nature. Although mathematically this appears to be a problem, it can be argued that the distribution of correlation functions measured in a real experiment is the valid distribution. The interpretation of the correlation function is another issue that brings back a long-standing discussion of whether turbulence consists of uncorrelated small eddies or large vortical structures of significant spatial coherence. If the turbulence is described by the former then the $<\rho vv, p'>$ correlation function measured from various points in the jet are mutually independent; the integration over the jet volume becomes a simple addition in power and the correlation data can be used to determine source efficiency along the jet axis (Seiner & Reethof, 1974). Such an interpretation also leads to a discussion of the number of eddies responsible for sound generation at a given instant (Lee & Ribner, 1972). It is now well established from various experimental observations that low Strouhal frequency turbulent fluctuations are dominated by the Kelvin-Helmholtz instability waves with significantly long spatial coherence. The effect of source-coherence on jet noise has been discussed by Michalke (1983). For sources with long coherence length scales the phase of $<\rho vv, p'>$ correlation will vary from point to point and the integration over the jet volume requires a knowledge of both magnitude and phase.

So far discussions have been confined to the contribution from the ρvv term only. It is straightforward to extend this analysis to include the second term of T_{ij} tensor, equation 1. The far field pressure fluctuations caused by pressure and density fluctuations in the plume are:

$$p'(\mathbf{X_f}; t) = \frac{1}{4\pi a_0^2 \, \mathbf{r}} \int_V \frac{\partial^2}{\partial t'^2} \left[\left[p' - a_0^2 \rho' \right] (\mathbf{X_s}; t') \right] d^3 \mathbf{X_s} . \quad (8)$$

To completely evaluate this term one needs to measure at least temperature and density fluctuations inside the plume. The present experimental setup is unable to do the former. Neglecting contribution from entropy fluctuations, local sound speed a_s relates pressure fluctuations to density fluctuations: p' = a_s^2 ρ'. Since $a_s^2 / a_0^2 = T_j / T_0$, where T_j is jet temperature and T_0 is ambient temperature, the above equation becomes:

$$p'(\mathbf{X_f}; t) = \frac{1}{4\pi \, \mathbf{r}} \int_V \frac{\partial^2}{\partial t'^2} \left[\left\{ \frac{T_j}{T_0} - 1 \right\} \rho'(\mathbf{X_s}; t') \right] d^3 \mathbf{X_s} . \quad (9)$$

where T_0 is the ambient temperature. For an unheated low Mach number jet $T_s / T_0 \approx 1$ and the right hand side has negligible contribution to the far field. However, as the Mach number M increases the effectiveness of this term is expected to increase as M^2. A reasonable estimate may be obtained by using time average plume temperature:

$$p'(\mathbf{X_f}; t) = \frac{\left(\frac{T_j}{T_0} - 1 \right)}{4\pi \, \mathbf{r}} \int_V \frac{\partial^2}{\partial t'^2} \left[\rho'(\mathbf{X_s}; t') \right] d^3 \mathbf{X_s} . \quad (10)$$

Once again, multiplying the source integral with the far field pressure fluctuations:

$$\left\langle p'^2 \right\rangle (\mathbf{X_f}; \tau) = \frac{\left(\frac{Tj}{T_0} - 1 \right)}{4\pi \, \mathbf{r}} \int_V \frac{\partial^2}{\partial \tau^2} \left[R_{\rho; p'}(\mathbf{X_s}, \mathbf{X_f}; \tau) \right] d^3 \mathbf{X_s}$$

$$\text{where,} \, R_{\rho; p'}(\mathbf{X_s}, \mathbf{X_f}; \tau) = \left\langle \rho'(\mathbf{X_s}; t + \tau - \tau_0) \, p'(\mathbf{X_f}; t) \right\rangle \quad (11)$$

Since data analysis is performed in narrowband frequencies, Fourier transform of above yields:

$$S_{p'2}(\mathbf{X_f}; f) \, df =$$

$$\left(1 - \frac{T_j}{T_0} \right) \frac{\pi f^2 df}{r} \, Re \left\{ \int_V S_{\rho, p'}(\mathbf{X_f}, \mathbf{X_s}; f) \, d^3 \mathbf{X_s} \right\} \quad (12)$$

$$\text{cross} - \text{spectrum:} \, S_{\rho, p'}(\mathbf{X_f}, \mathbf{X_s}; f) =$$

$$\int_{-\infty}^{\infty} R_{\rho; p'}(\mathbf{X_s}, \mathbf{X_f}; \tau) \exp(-j 2\pi f \tau) \, d\tau$$

Therefore, a correlation between the flow density fluctuations and the far field sound pressure fluctuations provides an estimate of contribution from the second term of Lighthill's stress tensor.

It is best to present the experimental data in a non-dimensionalized form. Following the traditional acoustic analogy approach, two different velocity scales are applied: ambient sound speed a_0 for field points and U_j for source points. The length and time scales are derived using the jet diameter D. Ambient value ρ_0 is used to normalize density. Using superscript * for non-dimensionalized quantities, S_t for Strouhal number, and M_a for Mach number based on ambient sound speed, equation 6 becomes:

$$S_{p'2}^*(\mathbf{X_f^*};S_t)\,dS_t =$$

$$-M_a^4\,\frac{\pi S_t^2}{r^*}\,dS_t Re\left\{\int_V S_{\rho vv,p'}^*(\mathbf{X_f^*},\mathbf{X_s^*};S_t)\,d^3\mathbf{X_s^*}\right\},$$

$$S_t = \frac{fD}{U_j}, \quad M_a = \frac{U_j}{a_0}, \quad S_{p'2}^* = \frac{S_{p'2}}{(\rho_0 a_0^2)^2\left(\dfrac{D}{U_j}\right)}, \qquad \textbf{(13}$$

$$S_{\rho vv,p'}^* = \frac{S_{\rho vv,p'}}{(\rho_0 U_j^2)(\rho_0 a_0^2)\left(\dfrac{D}{U_j}\right)}$$

Similarly, non-dimensionalized contribution from the second term (equation 12) is:

$$S_{p'2}^*(\mathbf{X_f^*};S_t)\,dS_t =$$

$$\left(1-\frac{T_j}{T_0}\right)M_a^2\,\frac{\pi S_t^2}{r^*}\,dS_t Re\left\{\int_V S_{\rho,p'}^*(\mathbf{X_f^*},\mathbf{X_s^*};S_t)\,d^3\mathbf{X_s^*}\right\},$$

$$S_{\rho,p'}^* = \frac{S_{\rho,p'}}{(\rho_0 a_0)^2\left(\dfrac{D}{U_j}\right)} \qquad \textbf{(14)}$$

In the present experimental program the principle idea of correlating flow fluctuations to the sound pressure fluctuations has been extended to include some other variables, which do not necessarily abide by the framework of Lighthill's equation. For example, efforts are made to correlate ρvv fluctuations not only with microphone signal from a 90° to jet axis but to a 30° position as well. Inquires are made as how do various other quantities, such as v, $\overline{\rho vv}$, $\rho'vv$ correlate with sound pressure fluctuations. These additional efforts resulted into some interesting results.

Fundamentals of flow measurement using Rayleigh scattering principle:

A simplistic description of the measurement process, using laser induced Rayleigh scattering is schematically shown in Fig. 2. When a laser beam is allowed to pass through a gas, the molecules present in the gas cause inelastic and elastic light scattering (Miles et. al. 2001).

The inelastic part is called Raman scattering and the elastic part Rayleigh scattering. The Rayleigh scattering process describes most (~ 99%) of the molecular scattered light. In the present experiment scattered light is collected and spectrally resolved to measure velocity. Since the Doppler shift frequency is relatively small, a narrow line width incident laser beam is necessary to resolve Rayleigh spectrum. Even if the gas medium is stationary, the random thermal motion of the gas molecules creates a wide range of Doppler shift - resulting in a spectral broadening of the collected light. The Full Width at Half Maximum (FWHM) depends on the spread of molecular motion and, therefore, is a measure of gas temperature. In the case of a moving gas media, the bulk motion is superimposed on the random velocity of the individual molecules; therefore separation between the peaks of the incident laser line and the Rayleigh spectrum provides a measure of the bulk velocity. Finally, the total light under the Rayleigh spectrum is proportional to the molecular number density and provides a measure of gas density. A single Rayleigh spectrum carries information of one component of gas bulk velocity, temperature and density.

This basic principle has been used in the past to measure *time-averaged* quantities (Panda & Seasholtz 1998, Forkey, Lempert & Miles 1998, Elliott & Sammimy 1996). Since density variation modulates the total scattered light, unsteady density fluctuations are easier to measure (Panda & Seasholtz, 2000, 2002 among others). Extension of the Rayleigh scattering technique to measure *unsteady* velocity fluctuation has remained a challenge. Recently, Seasholtz, Panda & Elam (2002) have simultaneously measured the time variation of density and velocity fluctuations in free jets. Earlier efforts that culminated towards the present setup can be found in Seasholtz, Panda & Elam (2001) and Seasholtz & Panda (1999, 2000). The present setup is for a point-measuring system; a continuous wave laser was used, and scattered light from a point on the beam was collected and analyzed. (It was realized early on that the current limitations of tunable pulsed-lasers and camera systems make an area measurement technique unsuitable for dynamic measurements over a large frequency bandwidth.) The scattered light collected from the probe volume was spectrally resolved by a Fabry-Perot interferometer. To illustrate the approach, first the nature of a fringe formed by the interferometer is shown in Fig. 3. The field of view in the image covers a fraction of the free spectral range. The narrow line width of the laser makes a sharp, narrow ring in the image. In contrast when the Rayleigh scattered light from a moving gas medium is imaged, a larger diameter diffused ring results. The radial shift in the peak intensity location corresponds to the Doppler shift associated with the bulk motion of the air stream, while the diffused image is

associated with thermal broadening. To measure time variation of the bulk velocity the variation of the ring diameter needs to be monitored. Seasholtz et. al. (2001, 2002) accomplished that through the use of an image dissector that split the image into two concentric parts (Fig. 4) and measured the ratio of light intensity from the inner and the outer parts using two photo-multiplier tubes. A calibration of the intensity ratio from known jet velocities was necessary for later use in unknown flows.

Fig. 5(a) presents a scattering diagram pertinent to the present optical and microphone setup. $\mathbf{k}_i$ is the incident wave vector normal to the jet flow direction, $\mathbf{k}_s$ is the scattered wave vector pointing towards the collection optics and, $\mathbf{k} = \mathbf{k}_s - \mathbf{k}_i$, is the scattering vector. The arrangement measures Doppler shift, $f_d = \mathbf{k}.\mathbf{U}/2\pi$ from the radial velocity component v. The optical frequency spectrum of Rayleigh scattered light $\Re(v-v_0)$ is closely related to the velocity distribution of the gas. For a low density gas the spectrum is given as:

$$\Re(v-v_0)\,df =$$

$$\frac{2\sqrt{\pi}}{a_p k}\exp\left[-\left\{\frac{2\pi(v-v_0)-\mathbf{k}.\mathbf{U}}{a_p k}\right\}^2\right]df \quad \textbf{(15)}$$

where, v_0 is the laser frequency and a_p, the "most probable molecular speed," is related to the local sound speed a and ratio of specific heat γ through $a_p=(2/\gamma)^{1/2}a$. The image formed, after the Rayleigh light is passed through a Fabry-Perot interferometer, is basically a convolution of the Rayleigh spectrum with the instrument function $I_{FP}(v, \theta_r)$. The light power distribution P_I at any position (r, θ) in the image plane is given as:

$$P_I(r,\theta) = P_\Re \iint \Re(v)\,I_{FP}(v,\theta_r)\,dv\,dA \quad \textbf{(16)}$$

where, $P_\Re$ is the total Rayleigh scattered power, and θ_r is the angle made by a light ray reaching the elementary area dA in the image plane with optical axis.

For a fixed optical setup and a fixed composition of gases the total scattered light is directly proportional to the gas density: $P_\Re \propto \rho$. The present experiment uses photon-counting electronics to measure light intensity. About 10% of the collected scattered light was split away and measured by PMT1 (Fig. 5c). If the count rate from PMT1 is N_1 then:

$$N_1 = C_{\rho 1} + \rho C_{\rho 2}\,, \quad \textbf{(17)}$$

where, $C_{\rho 1}$ and $C_{\rho 2}$ are calibration constants. The rest of the light was passed through the interferometer, the image formed at the focal plane of the fringe-forming lens was dissected into two parts by a concentric, tilted mirror assembly (image dissector in Fig. 5c) and measured by two PMT. It was found that for small velocity fluctuations (<150m/s) the light intensity in either part of the dissected image is directly proportional

to velocity. If N2 and N3 denotes the count rate from the inner and outer PMTs then:

$$N_2 = C_{in\,1} + v\,C_{in\,2}\,, \quad N_3 = C_{out\,1} + v\,C_{out\,2} \quad \textbf{(18)}$$

where, C_{in1}, C_{in2}, C_{out1} and C_{out2} are calibration constants. The radial velocity v is measured from a ratio of the two counts, $R=N_3/N_2$:

$$v = \frac{C_{out\,1} - RC_{in\,1}}{RC_{in\,2} - C_{out\,2}} \quad \textbf{(19)}$$

Note that the ratio of two counts $R=N_3/N_2$ cancels out changes in overall scattering intensity associated with flow density variation. The above analysis does not account for changes due to temperature fluctuations on Rayleigh spectra. A numerical uncertainty analysis (Seasholtz et. al. 2001), however, demonstrates that such an effect is small compared to the bigger change associated with velocity fluctuations.

Density (Favre) weighted velocity fluctuation: In numerical simulation of compressible flow, such as in Large Eddy Simulation (LES) it is customary to perform a density-weighted filtering of all variables; for example, radial velocity becomes:

$$\tilde{v} = \frac{\overline{\rho\,v}}{\overline{\rho}} \quad \textbf{(20)}$$

where the over-bar represents a time averaging and the ~ represents density weighting. The effect of the latter has not been verified experimentally. The availability of both density and radial velocity data has been used to check modifications induced by such a procedure.

II. EXPERIMENTAL SET-UP

Experiments were performed at NASA Glenn Research Center using three different nozzles (one convergent and two convergent-divergent) operated at Mach numbers, M = 0.95, 1.4 and 1.8. The convergent-divergent nozzles were designed by the method of characteristics and their geometries were reported in Panda & Seasholtz (1999a). All nozzles were 25.4 mm in exit diameter. The jet facility used a continuous supply of unheated compressed air. The facility was located in a large test chamber, which was not anechoic per se, but acoustic absorbent material was placed around the vicinity of the nozzle and in the ceiling and walls of the test cell to minimize reflection. Two 1/4-inch microphones were used to measure sound pressure fluctuation spectra. One of the microphones was located at 30° to the jet flow direction and the other at 90° (Fig. 1). While the 30° microphone was stationary at 50 diameters away from the nozzle exit, the 90° microphone was moved with the laser probe volume to ensure correct matching of direction cosines between the measured velocity component v, and the microphone location $\mathbf{X}_f$ (equation 4). The Rayleigh scattering system is somewhat elaborate and the following provides a description.

An in-depth discussion of the Rayleigh set-up can be found in Seasholtz, Panda & Elam (2001, 2002). Following is a brief discussion of some of the central features. The optical system was built in two parts. The first one is around the jet facility for transmitting laser light and collecting the scattered light (Fig. 5b). The scattered light was then passed through 0.55mm diameter optical fiber to a quiet room where the second part, consisting of spectroscopic and photon counting electronics, were placed (Fig. 5c). The splitting of the setup is a part of special attention that had to be taken for successful implementation of the optical setup. Care had to be taken to reduce dust particles in the air streams, to minimize the effect of vibration on the optical equipment and to stabilize the interferometer from temperature and vibration induced drifts. To reduce dust particles the dry air, supplied to the rig from a central high-pressure facility, was passed through sub-micron filters. This made the primary jet air very clean. To clean the entrained ambient air, an additional air blower & filter system was installed that provided a large, 200mm diameter, clean co-flow around 25.4mm primary jets. The optical system around the jet facility was built over an X-Y traversing unit that carried laser head, transmission and collection optics. The probe volume was moved from point to point in the plume, and thereby, allowing survey over a cross-sectional plane. To maximize utilization of the available light the laser head of the solid-state, frequency-doubled, Nd:VO$_4$ laser was placed at the bottom part of the set-up (fig. 5b). About 5 watts of single mode, 532nm-wavelength laser light was transmitted through a hollow side beam that contained a half-wave plate, focusing lens, mirrors and baffles. Since Rayleigh scattered light is polarization dependent, the half-wave plate was rotated to align the peak scattering plane with receiving optics. The background scattered light was significantly attenuated by suitable use of baffles and beam-dump. The laser head was placed in the same traversing unit as the rest of the transmission and collection optics. It was found that the noise from the jet created a tonal excitement of the laser line at around 450Hz. To reduce this excitation an anechoic box was built around the laser head. This box significantly reduced the laser unsteadiness, but a trace remained and it has manifested in the experimental results. The Rayleigh scattered light was collimated by a 300mm focal length and 80mm diameter achromat and focused by a 160mm focal length achromat on the face of a .55mm diameter multimode fiber. The combination of the fiber diameter and the magnification ratio of the collection optics fixed the probe volume length to 1.03mm. The beam waist was about 0.16mm^2 in diameter. An additional part of the set-up (not shown in fig. 5b) is collection of a small part of light from the transmitting beam for the purpose of monitoring laser

frequency as well as to maintain a close-alignment in Fabry-Perot interferometer. Whenever necessary, a pneumatically actuated mirror was placed in the transmission laser path to divert light towards a diffuser. The diffuser was simultaneously brought in front of the collection fiber and reference light, instead of the Rayleigh scattered light, was passed through the collection fiber.

To protect the spectroscopic equipment and the split mirror assembly from high noise level generated by supersonic jets, they were separately kept in an adjoining quiet room. This second part of the setup is schematically shown in Fig. 5(c). Light arriving via optical fiber was collimated by 100mm focal length lens L1, and about 10% was split by BS1 and measured by PMT1. Output from PMT1 provided information on the modulation of total scattered light intensity and therefore, was proportional to the air density fluctuations. The rest of the collimated beam was passed through a 70mm aperture Fabry-Perot interferometer for spectral analysis. Ideally, single wavelength light from an extended source is imaged as consecutive rings (fringes) at the output of the interferometer. However, restriction of field of view, imposed by the fiber diameter, created only one fringe as shown earlier in Fig. 3. The fringe-forming lens, which ultimately images the fiber face on the image dissector, was made of two 35mm camera lenses with suitable separation for an effective focal length of 2727mm. The large magnification ratio of the setup created a 15mm diameter image of the fiber on image dissector. The image dissector was made of two concentric, and slightly tilted mirrors. The inner one had a diameter of 10mm and directed the inner part of the fringe to PMT2, while the 25mm diameter outer one directed the outer part of the fringe to PMT3. The ratio of light intensities from PMT2 and PMT3 provided a measure of radial component of velocity as described earlier.

The success of the velocity measurement system is critically dependent on stable operation of the interferometer. Slight thermal drift or change in the incident laser frequency displaces the reference fringe (fig. 3a) and manifests as an artificial bias in velocity measurement. This makes the auto-alignment setup (fig. 5c) a necessary part. The alignment system is basically a feedback control that first measures the reference fringe diameter and compares it with a prescribed targeted size. This part is accomplished by splitting parts of the transmitted light using a 3-prism assembly, and imaging them on a CCD camera. Subsequently, the difference between the targeted to the measured fringe diameter is translated into a change of high voltage supply to the piezo-electric actuators that adjust interferometer's plate separation. Before every Rayleigh measurement, reference light was collected, passed through the same

fiber and optical system, and the auto-alignment system was engaged. When the desired fringe diameter is obtained within a tolerance, the reference light collection system around the jet facility and the prism assembly were disengaged, and velocity and density measurement via analysis of Rayleigh scattered light began.

Photoelectron counting electronics were used with all 3 PMT signals. The counting was performed over contiguous bins of prescribed time-duration. The digitization of the microphone signals was synchronized and finally 3 channels of photoelectron count and 2 channels of microphone signals were simultaneously acquired in a Personal Computer, which also controlled all other aspects of the operation. Long time records of up to 5 million data points from each PMT and microphone channels were acquired with a sampling rate between 25,000 to 40,000 samples/sec. The data points were converted to physical parameters: instantaneous density, velocity and sound pressure through the usage of proper calibration constants. The Welch method of modified Periodograms (1967) was used to calculate individual spectrum and cross-spectral density. Each long record was divided into small, 50% overlapped, segments; modified periodograms of each segment provided local estimates; average of all local estimates provided the final cross-spectral density. The cross-spectra were normalized by pertinent individual spectra to obtain coherence function.

III. RESULTS:

For the calibration of three PMT signals a separate small nozzle facility was mounted close to the laser probe volume. The calibration jet was rotated to align along the radial velocity direction of the primary jet. Fig. 6. shows a set of typical calibration curves for density and radial velocity measurement. The calibration constants required in equations 17 & 18 were calculated from least-square fits to the experimental data. The linear relation between velocity variation and photon count from either of the inner or outer PMTs is confirmed from this figure. The calibration process usually took better part of a working day. Therefore, jet plume data could not be acquired on the same day. The laser frequency and Fabry-Perot setup showed a slight drift, which was significant enough to add a fixed time-average value to the radial velocity measurement. Data from the jet centerline, where time average v is expected to be zero, is found to drift away significantly. Therefore, time-averaged velocity was always subtracted from the instantaneous quantity before calculating the ρvv product. This is believed to be reasonable as time-averaged radial velocity is expected to be small in fully expanded jets.

Density and velocity fluctuations spectra: Figures 7 and 8 show typical velocity and density spectra obtained

from respectively, peripheral shear layer, and centerline of all plumes tested. All velocity data is non-dimensionalized by the centerline axial velocity U_j while density is non-dimensionalized by the ambient value[1]. Along the shear layer radial velocity and density spectra have similar shapes with humps around the most energetic frequency. Data from the centerline, however, shows a distinct difference: while v-spectrum has a hump shape, the density spectrum shows a continuously decaying shape - indicating the most energetic fluctuations always occurring at the lowest frequency. Various models for turbulent fluctuations assume the same spectral form for both velocity and scalar fluctuations. The experimental data shown in figs. 7 & 8 show that such an assumption is valid in the outer shear layer and invalid at the jet core.

The density-weighted velocity is compared with the straightforward velocity spectra in Figs. 7(b) and 8(b). In spite of the difference between the ρ' and v' spectra, the shape of $\rho'v'/\bar{\rho}$ spectra is similar to that of velocity in both figures. The spectral levels, however, are significantly increased. The similarity in the spectral shape is somewhat expected, as the absolute value of mean-square density fluctuation is weaker than that of velocity fluctuations. Following is a discussion of measurement uncertainty.

The fundamental source of uncertainty in optical measurement is due to electronic shot noise. This noise has a Poisson distribution, which dictates that the variance of photoelectron count is equal to the mean. Since density spectra are calculated directly from Fourier transform of photoelectron counts, the effect of electronic shot noise is determinable. A detailed discussion of the effect of shot noise on density spectrum is provided in Panda & Seasholtz (2002). In essence, shot noise adds a constant floor as well as a randomness in density spectra. The latter is significantly reduced in the present experiment by averaging over many segments obtained from 3 to 5 million points long data string. The constant noise floor particularly masks the lower energy, high-frequency side of the spectrum. Panda and Seasholtz (2002) used a 2-PMT-correlation technique to alleviate this problem. In the present work no such correlation technique is applied. It is estimated that as much as 30% of spectral energy at $St = 0.5$ may be due to this electronic noise source.

---

[1] In the earlier publication (Panda & Seasholtz 2002), density was non-dimensionalized by the difference between the jet core and ambient densities, which perhaps is more logical from mixing point of view. The current choice of ambient density, however; is based upon Lighthill's' and prior work on causality relation.

The propagation of electronic shot noise in the velocity spectrum is somewhat complicated by the ratio of photoelectron counts, $R = N_3/N_2$, (representing a ratio of light intensity from inner and outer PMTs, equation 19) needed to determine instantaneous velocity. The shot noise randomly changed the ratio from that caused by velocity fluctuation and is manifested as a noise floor in the velocity spectrum. There are three other sources of noise in velocity data. First, a slow random variation in the laser frequency over 30 MHz (.001 cm^{-1}) that translates into ±8m/s velocity fluctuation. Second, a periodic variation of the laser frequency at about 450Hz induced by the intense sound level produced by the jet. As described earlier the laser head was enclosed in an anechoic box to alleviate this problem. Nevertheless, the periodic variation could not be completely eliminated. The velocity fluctuations spectra in figures 7(b) and 8(b) show large spurious peaks at this frequency. Finally, the Fabry-Perot stabilization setup, needed to lock the reference fringe at a fixed radial position, was effective only within an error margin. A change in the reference fringe position, from the value used for calibration, translates into a spurious mean velocity in the analyzed signal. Similarly, a random positioning error in reference fringe results in added energy in the spectral data. A direct estimate of the uncertainty from all such sources is difficult to obtain. Seasholtz, Panda & Elam (2002) provides a comparison between velocity spectra measured by the present Rayleigh scattering technique and a hot-wire probe in low speed jets. The shape of the spectrum were found to be similar in both cases, while the absolute energy level in the velocity spectrum measured by the Rayleigh technique is found to be two times of that from hot-wire. Such a discrepancy is expected since almost all noise sources contribute towards increasing the spectral floor. In general, the signal to noise ratio improves with increasing jet velocity as the noise sources are mostly independent of jet speed. A factor of 2 increase in the spectral amplitude is the upper limit of experimental uncertainty in velocity spectral data. The contributions from various noise sources greatly affect the ρvv spectra, which for the most part, is inundated by noise. Nevertheless, the success of the causality method is critically hinged on noise cancellation obtained in cross-correlating two signals of independent noise sources. This cross-correlation is described in the next section. The primary source of uncertainty in the microphone spectra is caused by sound wave reflection from large optical components placed around the jet. The ripples seen in figure 8(d) are telltale signs of reflection. The 90° microphone was additionally affected by some reflection from a nearby, partially anechoic wall.

Correlation between flow fluctuations and sound pressure fluctuations: The presentation of correlation data starts with Fig. 9, where normalized cross-correlation plots for both 30° and 90° microphone are presented. The cross-correlation values were calculated via Fourier transform, that is, the cross-spectrum was calculated first, and then an inverse transform was taken to return back to the time domain. Neither of the flow data or microphone data were shifted in time. The cross-correlation data show sharp rise at a time delay τ_0, which is found to be the time needed for sound waves to travel from the laser probe location to the microphone location, $\tau_0 = \mathbf{r}/a_0$. This confirms that the "cause" (ρ, v, ρvv fluctuations in the jet) produces the "effect" (microphone pressure fluctuations) at a predictable time lag, and in turn provides confidence on the measured data. The laser probe location corresponds to the end of the potential core, which is known to be a strong sound source from various earlier measurements. There are multiple interesting observations made from Fig. 9. First, among all variables, it is air density fluctuations inside the jet that show the best correlation with the far-field noise at both 30° and 90° locations. In fact, the normalized correlation coefficients are nearly an order of magnitude higher than those obtained either from radial velocity v or from ρvv fluctuations. This is found to be consistent from all probe locations along centerlines and lip shear layers for all three Mach number jets. Second, fig. 9c shows that, contrary to the expectation from Lighthill's equation, ρvv fluctuations are uncorrelated with the sound pressure fluctuations at 90°-location; while there exists good correlation with the 30°-location. As discussed earlier, ρvv fluctuations reflect quadrupole sources radiating primarily 90° to the jet axis. In a stricter sense, it is the second time derivative of cross-correlation between ρvv and 90°-microphone that represents sound source. However, since the cross-correlation itself falls in the experimental noise level, there is no need for any derivative. The higher level of correlation between ρvv fluctuation and 30°-microphone signal can be reconciled in the following way. The acoustic analogy makes a component of ρuu fluctuations (u representing axial velocity component) the relevant source for 30° noise (Schaffer 1979, Ricarz 1979, Lee & Ribner 1972). Therefore, it can be concluded that ρuu and ρvv stress tensors are somewhat dependent. In fact this has been verified by numerous experimental studies of instability waves present in low-speed jets. For example, Hussain & Zaman (1981) show that the passage of an instability wave produces comparable fluctuations in both axial u and radial v velocity components. Further all 9 turbulent stresses, arising from the passage of coherent structures, are related. This has led to an effort to determine the effectiveness of

$<\rho vv, p'>$ correlation (measured using 30° microphone) in producing sound pressure fluctuations at 30° to the jet axis.

Contribution to 30° far field sound from ρvv fluctuations: Equation 13 describes that the contribution from ρvv fluctuations can be determined from a knowledge of the real part of $S_{\rho vv, p'}$ cross-spectrum. The nature of this relationship from a single point measurement is examined in Fig. 10. The laser probe location is the same as in the previous figure and corresponds to the strongest sound-emitting region in Mach 1.4 plume. Among various intermediate steps the critical component is the calculation of the real part of the cross-spectrum in fig. 10(b). For correct calculation the microphone time signal had to be shifted by propagation delay; otherwise a phase factor is introduced which varies with frequency. The correct choice of the delay time leads to a minimum phase variation across the complete frequency range (fig. 10c). Finally, a multiplication by frequency^2 and the additional factors of right hand side of equation 13 result in fig. 10(d). Physically, fig. 10(d) represents contribution to the sound auto-spectrum from a unit volume (diameter^3) around the probe location. Note that the ordinates of figs 10(d) and 10(e) differ by a factor of 10. Therefore about 1% of noise at St=0.2 is attributable to ρvv fluctuations at the probe location. The experimental uncertainty in the calculated spectra of Fig. 10(d) is frequency dependent, which is discussed in the following.

As mentioned earlier, the ρvv spectrum is submerged in instrumentation noise, however, the ρvv-p' cross-spectrum is expected to be benefited from significant cancellation, as sources of uncertainty in ρvv measurement are absent in microphone measurement. Figure 10(a) indeed shows that is correct. A numerical simulation using two synthetically generated signals of similar time duration as the present data and comparable noise levels seen in ρvv and p' measurements shows that the noise floor in cross-spectral magnitude is reduced by a factor of 10^5. Now, evaluation of equation 13 requires using the real part of cross-spectrum and multiplication by frequency^2. Since cross-spectral phase is slower to converge, the real part of the spectrum becomes noisier at the higher frequency end. A lack of convergence makes the phase oscillate between +ve and –ve values, leading to a similar oscillation in the real part. Multiplication by frequency^2 further worsens this oscillation. It is known that acoustic spectrum, along the peak mixing noise direction, increases as frequency^2 at the low frequency end, while the high frequency end decreases as frequency^{-2}. Therefore, to be able to resolve the high frequency side, the real part of the $<\rho vv-p'>$ cross-spectrum has to behave as frequency^{-4}, which was

not the case in Fig. 10(b). The ultimate result is that beyond St = 0.3 calculated contribution towards the microphone auto-spectra is lost in instrumentation noise, while the small contribution at lower St end is still discernable.

Reynolds decomposition of density and its effect on ρvv-microphone correlation: Many existing jet noise prediction models assume flow density to be constant in evaluating the density*velocity*velocity product term, i.e., $\rho vv \approx \bar{\rho} vv$. All earlier studies employing the causality technique also used the same assumption. The present experimental technique allowed for an evaluation of this assumption in changing the nature of sound source. Towards this end the density*velocity*velocity product is created using total density ρ, time-averaged density $\bar{\rho}$ or the fluctuating part of density ρ'. In other words decomposition of density ρ into a time-average and fluctuating part $\rho = \bar{\rho} + \rho'$ lead to three different products ρvv, $\bar{\rho}$vv and ρ'vv. When these three products are individually cross-correlated with pressure fluctuations measured from a fixed 30° microphone, 3 different results are obtained (Fig. 11), and the results are also found to be Mach number dependent. First, the ρ'vv-p' cross-spectrum is opposite in phase to that of $\bar{\rho}$vv-p'. The resultant sum, which represents the correct quadrupole source, depends on the relative amplitude of these two competing components. For the lowest Mach 0.95 jet the contribution from ρ'vv-p' cross-spectrum is small and indeed the assumption of $\rho vv \approx \bar{\rho}$vv is found to be reasonable. However, as the jet Mach number increases, the density fluctuations become more vigorous and the above assumption falls apart. In the highest Mach 1.8 jet, the real part of ρ'vv-p' cross-spectrum nearly cancels out that from $\bar{\rho}$vv-p' cross-spectrum, resulting in a weakening of the quadrupole source.

Contribution to far field sound from density fluctuations: Equation 14 describes that the contribution from density fluctuations can be determined from a knowledge of the real part of $S_{\rho, p'}$ cross-spectrum. The nature of this relationship from a single point measurement is examined in Fig. 12. The laser probe location and operating conditions are the same as used to determine the contribution from ρvv fluctuations in Fig. 10. However, unlike that data, the uncertainty level in $S_{\rho, p'}$ cross-spectrum is far less, simply because of an order of magnitude higher correlation from density fluctuation. Note that the calculated contribution in Fig. 12(d) is plotted in the same scale as the microphone auto spectra in fig. 10(e). A comparison shows that about 10% of jet noise at 30° to the microphone axis is attributable to an unit volume around the laser probe location. Further

exploration of relative contributions from ρvv-p' and ρ-p' cross-spectrum to the far-field noise in two different Mach numbers is shown in figure 13. Once again the microphone was kept at the peak mixing noise direction of 30° to the jet axis and 50 diameters from the nozzle lip, and equations 13 and 14 were used to estimate individual contribution from the first and second term of the Lighthill's equation. Note that the contribution from ρvv-p' correlation is multiplied by a factor of 10. Figure 12 shows that an increase in jet Mach number leads to an increased contribution from density fluctuation and a decreased contribution from ρvv fluctuation.

So far all correlation data are shown from a single point inside the jet. However, the causality relationships require an integral of correlation functions from various points in the entire jet plume. The outcome of integration depends on the coherence of ρ or ρvv fluctuation inside the jet. A long coherence length leads to a different cross-spectral phase and the sum needs to be evaluated for correct verification. Therefore, $S_{\rho,p'}$ cross-spectrum was measured from 7 different points along the jet axis (x/D = 2, 4, 6, 8, 10, 12 & 14)by moving the laser probe while keeping the microphone fixed at 30° and 50 diameters from the nozzle exit. With a simplifying assumption that the cross-spectral density does not change across the jet cross-section, equation 14 is evaluated as

$$S^*_{p'2}(\mathbf{X^*_f};S_t)\,dS_t = \qquad\qquad \textbf{(21)}$$

$$\left(1 - \frac{T_j}{T_0}\right)M_a^2\,\frac{\pi S_t^2}{r^*}\,dS_t\,\frac{\pi}{2}\sum_{\mathbf{X^*_s}=2}^{14}\mathrm{Re}\left\{S^*_{\rho vv,p'}(\mathbf{X^*_f},\mathbf{X^*_s};S_t)\right\}^{\cdot}$$

The result is shown in Fig.14. A comparison of the calculated spectrum with that of the microphone auto-spectrum shows that nearly a third of the sound power can be predicted from the above exercise. For exact comparison the integration had to be carried out over the entire jet plume and far more cross-spectral data had to be acquired. This however, was not attempted. Nevertheless, that a significant part of the mixing noise can be calculated from the measured density-sound pressure correlation is remarkable, and goes to demonstrate the usefulness of the causality method in determining sound sources.

Comparative study of correlation from various parts of Jets: Some of these comparative studies are already presented in the earlier figures. Figure 15 demonstrates the growth in the turbulence spectrum measured along the centerline of a Mach 1.8 jet. At x/D=4 the potential core was still present, and the spectral data is mostly due to instrumentation noise. The x/D=10 station lies around the end of the potential core where turbulence intensity is the largest; Further downstream at x/D = 16 the high

frequency part of the spectrum shows some decay. When data used for these spectra are correlated with far field microphone signals from 30° and 90° to the jet axis coherence values as shown in figure 16 are found. Coherence spectrum is obtained through non-dimensionalization of the cross-spectral data by individual power spectrum. For example, $S_{\rho vv,p'}$ cross-spectrum is normalized as:

$$\Gamma^2_{\rho vv,p'}(\mathbf{X_f},\mathbf{X_s};f) = \frac{S_{\rho vv,p'}}{\left|S_{\rho vv}\right|\left|S_{p'}\right|}\quad\textbf{(22)}$$

To distinguish between correlation from 30° and 90° microphones, the subscript p' is replaced by microphone azimuthal position: $\Gamma^2_{\rho vv,30°},\Gamma^2_{\rho vv,90°}$. Similarly, coherence functions $\Gamma^2_{\rho,30°},\Gamma^2_{\rho,90°}$ are also defined[2].

Once again, coherence data between ρvv fluctuations and noise measured by 90°-microphone, representing source correlation from a longitudinal microphone, is immeasurable. It falls below instrumentation noise floor. In general the 30°-microphone, located at the peak noise radiation direction, correlates better than that from the 90°-microphone. Density fluctuations show the highest correlation with far field noise. Note that the scale used to plot coherence between ρvv;p' coherence is 1/10th of that used to plot ρ;p' coherence. Data from the lower Mach 0.95 jet, in Figure 17 show similar behavior described above except for significantly lower coherence values.

IV. SUMMARY AND CONCLUSIONS:

A recent advancement in molecular Rayleigh scattering technique, to simultaneously measure velocity and density fluctuations in high-speed flows, has been utilized to identify sound sources in supersonic and high subsonic unheated free jets. The particle-free, non-invasive technique involves passing a narrow CW laser beam through jet plumes and the collection of molecular scattered light from various points on the beam. A part of the collected light is directly measured to detect fluctuating intensity, which is related to air density fluctuations via calibration constants. The rest of the collected light was passed through a Fabry-Perot interferometer to detect Doppler shift associated with one component of jet velocity. The Fabry-Perot was operated in an imaging mode and the fringe formed at the image plane was split into two parts. The ratio of

---

[2] In the earlier publication (Panda & Seasholtz 2002), square root of coherence spectra were plotted, that is, $\Gamma_{\rho,p'}$ instead of currently used $\Gamma^2_{\rho,p'}$.

light intensity was related to velocity using another set of calibration constants.

The current setup was built to measure the radial component of velocity v. Time histories measured from various points in the plume were Fourier transformed to obtain spectra. A comparison between density and velocity spectra shows that they are similar in the shear layer and different at the jet core. Favre-averaged velocity spectra, calculated from $\rho v / \bar{\rho}$ time histories, show a similar shape as that of velocity spectra, yet at an increased level of spectral energy.

The noise emitted by the jets was measured by 2 microphones placed nominally 50 diameters and 30° & 90° to the downstream direction. The microphone signals p' were correlated with ρ, v and ρvv signals measured from various points in the flow to determine sources of sound radiation. The non-intrusiveness of the laser-based technique avoids the probe-interference effects that have plagued previous attempts of source identification via causality method. The correlation data were interpreted via Lighthill's equation to determine effectiveness of the two source terms in generating far field noise. It is argued that the source point to field point correlation utilized in the causality formulation overcame a fundamental limitation of Lighthill's equation in separating radiating and non-radiating parts of disturbances. Some significant observations from this study are the following:
(a) Flow fluctuations are found to be significantly better correlated to the sound pressure fluctuations at 30° to the jet axis than from the 90°-location.
(b) Air density fluctuations in the jet are found to provide nearly an order of magnitude higher correlation than any other flow variables. When the correlation data is interpreted through the second source term in Lighthill's equation (with an assumption of negligible entropy fluctuations) nearly 10% of sound generated 30 deg to jet axis is found to be predictable from a single correlation measurement at the end of the potential core. The causality relationship dictates that sound pressure fluctuations is an integral of all correlations measured from the jet plume. An approximate estimate of this integral from various centerline measurements in Mach 1.4 jet shows that nearly 1/2 of the sound pressure fluctuations are predictable from density fluctuations alone.
(c) The ρvv fluctuations measured in the plume represent one of the quadrupole sources in the plume. The effectiveness of this source in producing far-field noise is identified via ρvv-p' correlation measurement. Unlike expectations from Lighthill's equation, the correlation is found to be zero within experimental uncertainty. However, ρvv is found to be better correlated with noise from 30°-location. It is ρuu

fluctuation, u being axial component of velocity, which is expected to be the source of 30°-noise. Prior experiment of the instability waves in low speed flow shows that u and v fluctuations caused by the passage of such a wave is related. Therefore various quadrupole terms, including those involving ρuu and ρvv, are expected to be related.
(d) The ρvv-p' correlation from the 30° microphone measured from a single point at the end of the potential core in Mach 1.4 jet is found to account for nearly 1% of noise at 30° location. Various analytical models and prior causality experiments have neglected density fluctuation in evaluating the ρvv product. It is found that such an assumption progressively falls apart as the Mach number increases. The ρvv-p' correlation differs by a factor of 3 from that of $\bar{\rho} vv$-p' in Mach 1.8 jet.
(e) The relative contribution from ρ-p' correlation is found to progressively dominate as the plume Mach number increases.
(f) The strongest sound-producing region is found to lie beyond the end of potential core. The <ρ-p'> correlations measured from the furthest x/D =16 station in Mach 1.8 plume shows significant coherence, indicating that the low frequency sources extend far beyond the end of the potential core.

The instrumentation noise limited the resolvable bandwidth in experimental data to St>0.6 for most of the correlation study. In addition, weak correlation caused limited success in identifying sources for sound pressure fluctuations at 90° to the jet axis.

References
Armstrong, R. R., Michalke, A. & Fuchs, H. V. 1977 Coherent structures in jet turbulence and noise. *AIAA J.* **15** (7), 1011-1017.
DeBonis, J. R. 2000 The numerical analysis of a turbulent compressible jet. *Ph. D. thesis, Ohio State University, also NASA TM 2001-210716.*
Elliott, G. S. & Samimy, M. 1996 Rayleigh scattering technique for simultaneous measurements of velocity and thermodynamic properties. *AIAA J.* **34** (11), 2346-2352.
Fedorchenko, A. T. 2000 On some fundamental flaws in present aeroacoustic theory. *J. Sound Vib.* **232**, 719-782.
Ffowcs Williams, J. E. 1973 Technical evaluation report. *AGARD CP 131 on Noise Mechanisms,* VII - XIX.
Forkey, J. N., Lempert, W. R. & Miles, R. B. 1998 Accuracy limits for planer measurements of flow field velocity, temperature and pressure using filtered Rayleigh scattering. *Experiments in Fluids,* **24**, 151-162.
Freund, J. B. 2001 Noise sources in a low-Reynolds-number turbulent jet at Mach 0.9. *J. Fluid Mech.,* **438**, 277-305.

Goldstein, M. E. 1976 *Aeroacoustics*, McGraw-Hill International Book Co., New York.

Hussain, A. K. M. F. & Zaman, K. B. M. Q. 1981 The 'preferred mode' of axisymmetric jet. *J. Fluid Mech.,* **110**, 39-71.

Lee, H. K., & Ribner, H. S. 1972 Direct correlation of noise and flow of a jet. *J. Acoustic. Soc. Of America.* **52**, no. 5 (pt. 1) 1280-1290.

Lighthill, M. J. 1954 On sound generated aerodynamically I. General theory. *Proc. Royal Soc.*, **A221** 564-587.

Lilley, G. M. 1972 The generation and radiation of supersonic jet noise IV. Theory of turbulence generated noise. USAPL TR-72-53.

Michalke, A. 1983 Some remarks on source coherence affecting jet noise. *J. Sound & Vib.* **87**(1), 1-17.

Miles, R. B., Lempert, W. R. & Forkey, J. N. 2001 Laser Rayleigh scattering. *Meas. Sci. Technol.* **12**, R33-R51.

Morris, P. J., Boluriaan, S., Lilley, G. M. & Long, L. N. 2002 Two-point cross correlations of turbulence and noise predictions: analysis and simulation. *AIAA paper no. 2002-0071*

Morris, P. J. & Tam, C. K. W. 1979 On the radiation of sound by the instability waves of a compressible axisymmetric jet. In *Mechanisms of Sound Generation in Flows* (ed. E. A. Muller). Springer.

Panda, J. & Seasholtz, R. G. 2002 Experimental Investigation of density fluctuations in high-speed jets and correlation with generated noise. *J. Fluid Mech.,* **450**, 97-130.

Panda, J., & Seasholtz, R. G. 1999a Velocity and temperature measurement in supersonic free jets using spectrally resolved Rayleigh scattering. *AIAA paper 99-0296.*

Proudman, I. 1952 The generation of noise by isotropic turbulence. *Proceedings of the Royal Society*, **A214** 119-132.

Rackl, R. 1973 Two causality correlation techniques applied to jet noise, *Ph. D. thesis, University of British Columbia.*

Richarz, W. G. 1980 Direct correlation of noise and flow of a jet using Laser Doppler. *AIAA J.* **18**(7), 759-765.

Schaffer, M. 1979 Direct measurements of the correlation between axial in-jet velocity fluctuations and far field noise near the axis of a cold jet. *J. Sound & Vib.* **64**(1) 73-83.

Seasholtz, R. G., Panda, J. & Elam, K. A. 2002 Rayleigh Scattering Diagnostic for Measurement of Velocity and Density Fluctuation Spectra. 40th AIAA Aerospace Sciences meeting, *AIAA paper no 2002-0827.*

Seasholtz, R. G., Panda, J. & Elam, K. A. 2001 Rayleigh Scattering Diagnostics for Dynamic Measurement of Velocity Fluctuations in High Speed Jets. *AIAA paper no 2001-0847.*

Seasholtz, R.G. & Panda, J. 2000 Rayleigh scattering diagnostic for simultaneous measurements of dynamic density and velocity," *AIAA paper 2000-0642.*

Seasholtz, R.G. & Panda, J. 1999 Rayleigh scattering diagnostic for dynamic measurement of velocity and temperature," *AIAA paper 99-0641.*

Seiner, J. M. 1974 The distribution of jet source strength intensity by means of a direct correlation technique. *Ph.D. dissertation, The Pennsylvania State University, Department of Aerospace Engr.*

Siddon, T. E. 1973 Noise source diagnostics using causality correlations, *AGARD CP 131, Noise Mechanisms* 7-1:7-13.

Seiner, J. M. & Reethof, G. 1974 On the distribution of source coherency in subsonic jets. *AIAA paper 74-4.*

Siddon, T. E. & Rackl, R. 1972 Cross-correlation analysis of flow noise with fluid dilatation as source fluctuation. *J. Acous. Soc. Amer.* **51** 96(A).

Tam, C. K. W. 2001 On the failure of the Acoustics Analogy Theory to identify the correct noise sources. *AIAA paper no 2001-2117.*

Tam, C. K. W. & Burton, D. E. 1984 Sound generated by instability waves of supersonic flows. Part 2. Axisymmetric Jets. *J. Fluid Mech.* **138** 249-271.

Welch, P. D. 1967 The use of fast Fourier transform for the estimation of power spectra: A method based on time averaging over short, modified periodograms, *IEEE Trans. on Audio and Electroacoustics,* **AU-15** 70-73.

Table I. Nominal Operating conditions:

Sp. heat ratio, γ = 1.4; Total temp., T_0 = 300°K; Ambient density, ρ_a = 1.16 Kg/m³, Ambient sound speed, a = 347 m/s

	Convergent operated at M = 0.95	M 1.4 CD	M 1.8 CD
Nozzle type			
Minimum shock operation at M =		1.395	1.795
Reynolds number Re_D	0.66x10⁶	1.16x10⁶	1.88x10⁶
Jet Velocity U_j (m/s)	316	411	486
Estimated eddy convection speed U_c (m/s) = $0.6U_j$ - $0.89U_j$	190 – 282	247-366	292-433
Jet density ρ_j (kg/m³)	1.36	1.6	1.89
Frequency (kHz) for Sr = 1	12.4	16.2	19.1
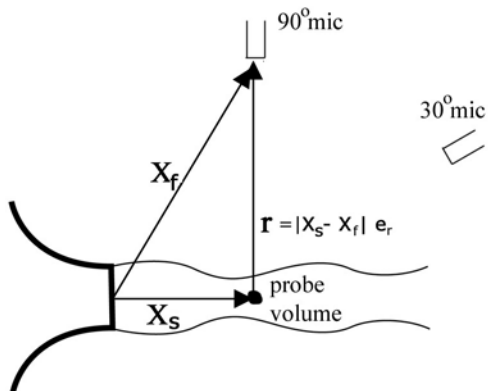
Fig. 1. Schematic of coordinate system and microphone locations.
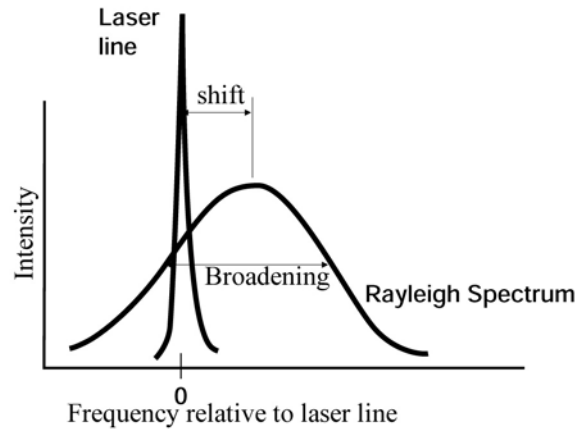
Fig. 2. Principle of Rayleigh scattering technique.
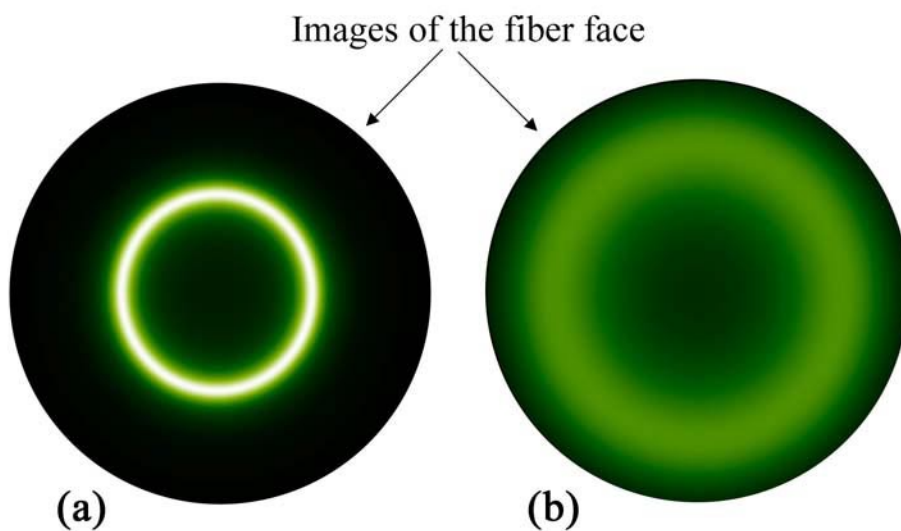
Fig. 3. Fringes formed after passing through Fabry-Perot Interferometer by (a) incident laser light (b) Rayleigh scattered light.
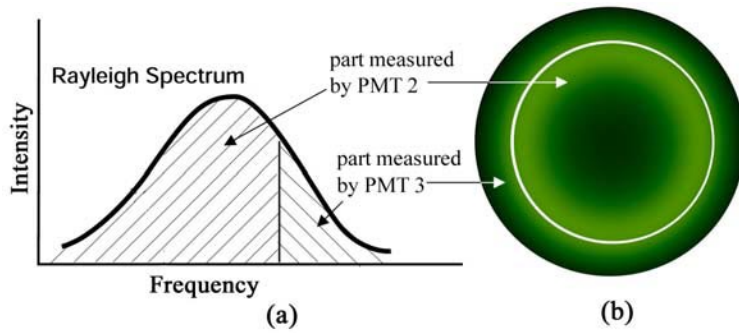
Fig. 4. Principle of instantaneous velocity measurement by Rayleigh scattering technique.

(a)

(b)

(c)
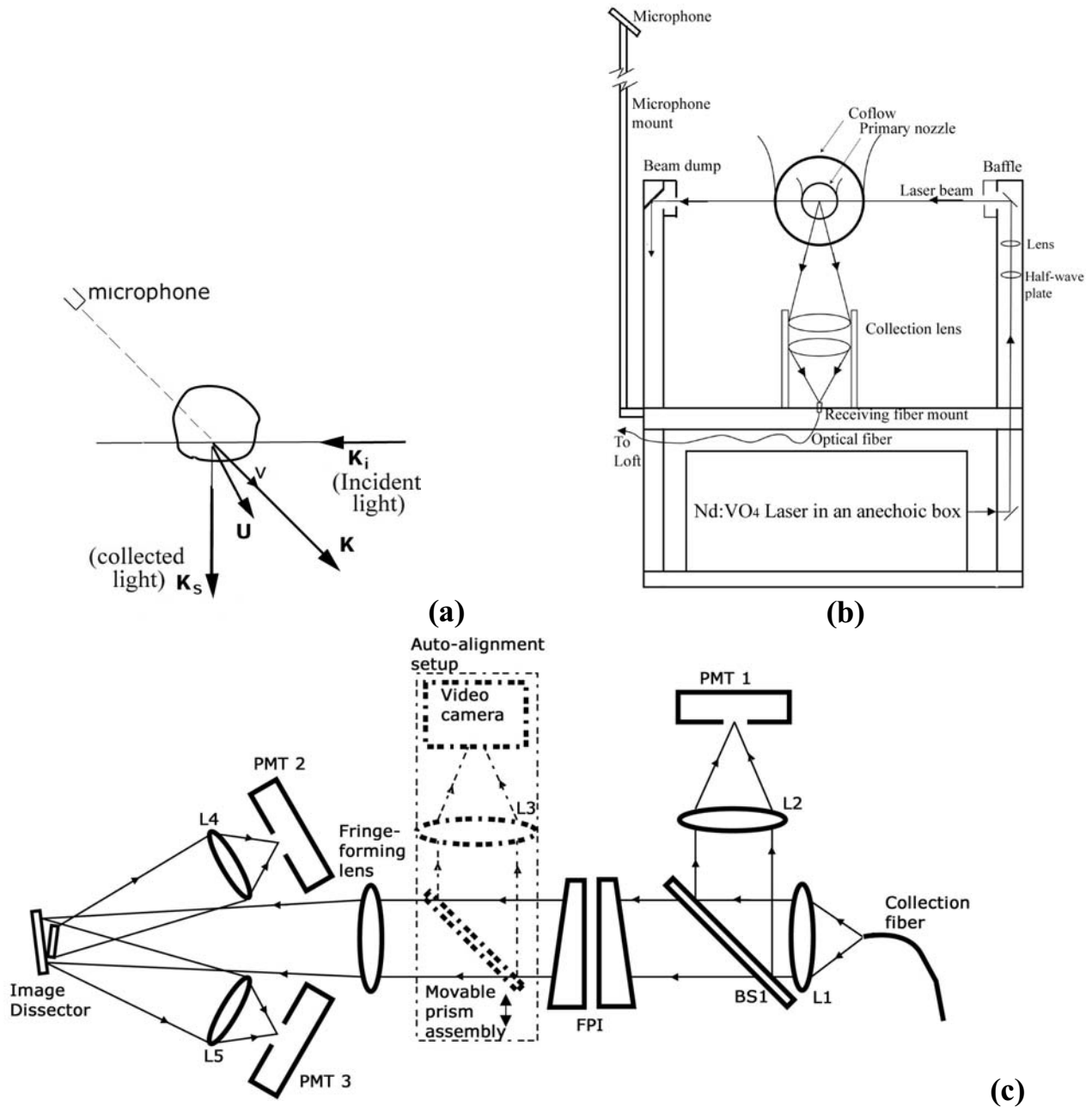
Fig. 5. (a) Scattering diagram for Rayleigh setup and 90° microphone azimuthal position. (b) Schematic of optical arrangement (mounted on X-Y traverse, not shown) around jet facility. (c) Schematic of optical setup in a quiet, adjoining room to analyze collected light. L1 to L5 are lenses; BS1 is beam-splitter and FPI is the Fabry-Perot interferometer.
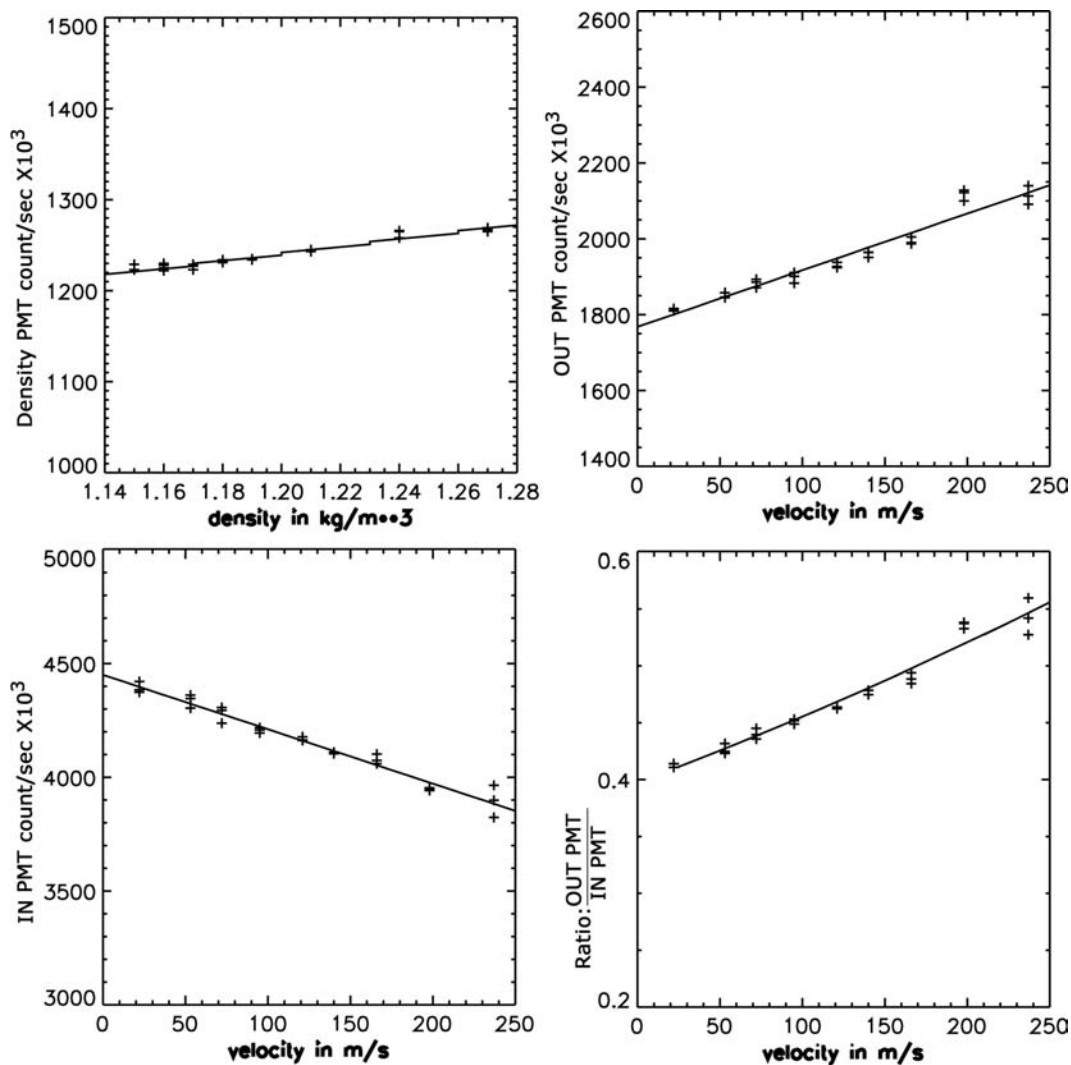
Fig. 6. Density and velocity calibration using 3 photo-multiplier tubes.
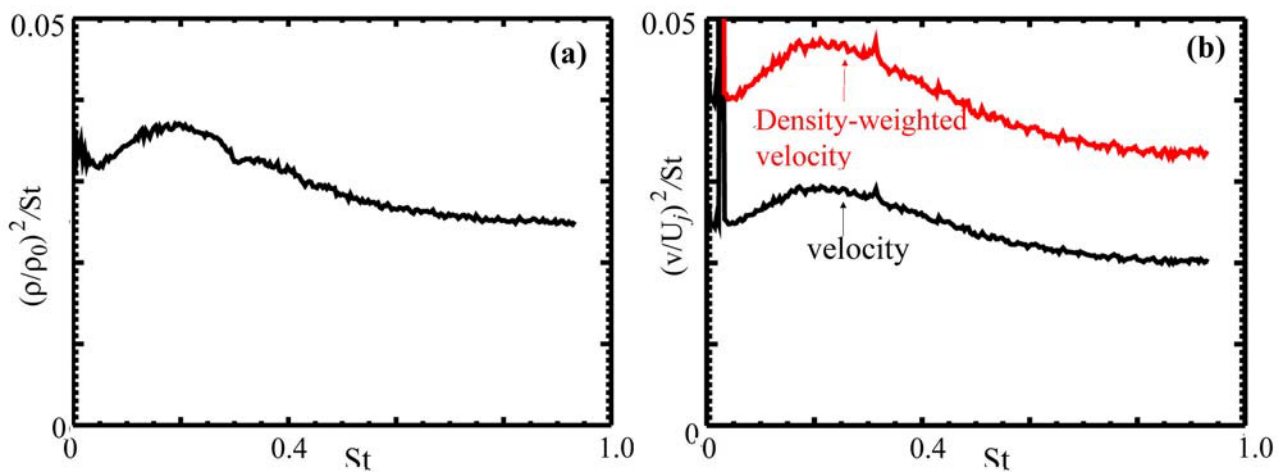
Fig. 7. (a) density & (b) velocity fluctuation spectra measured from x/D=8, r/D=0.48 of Mach 1.4 jet.
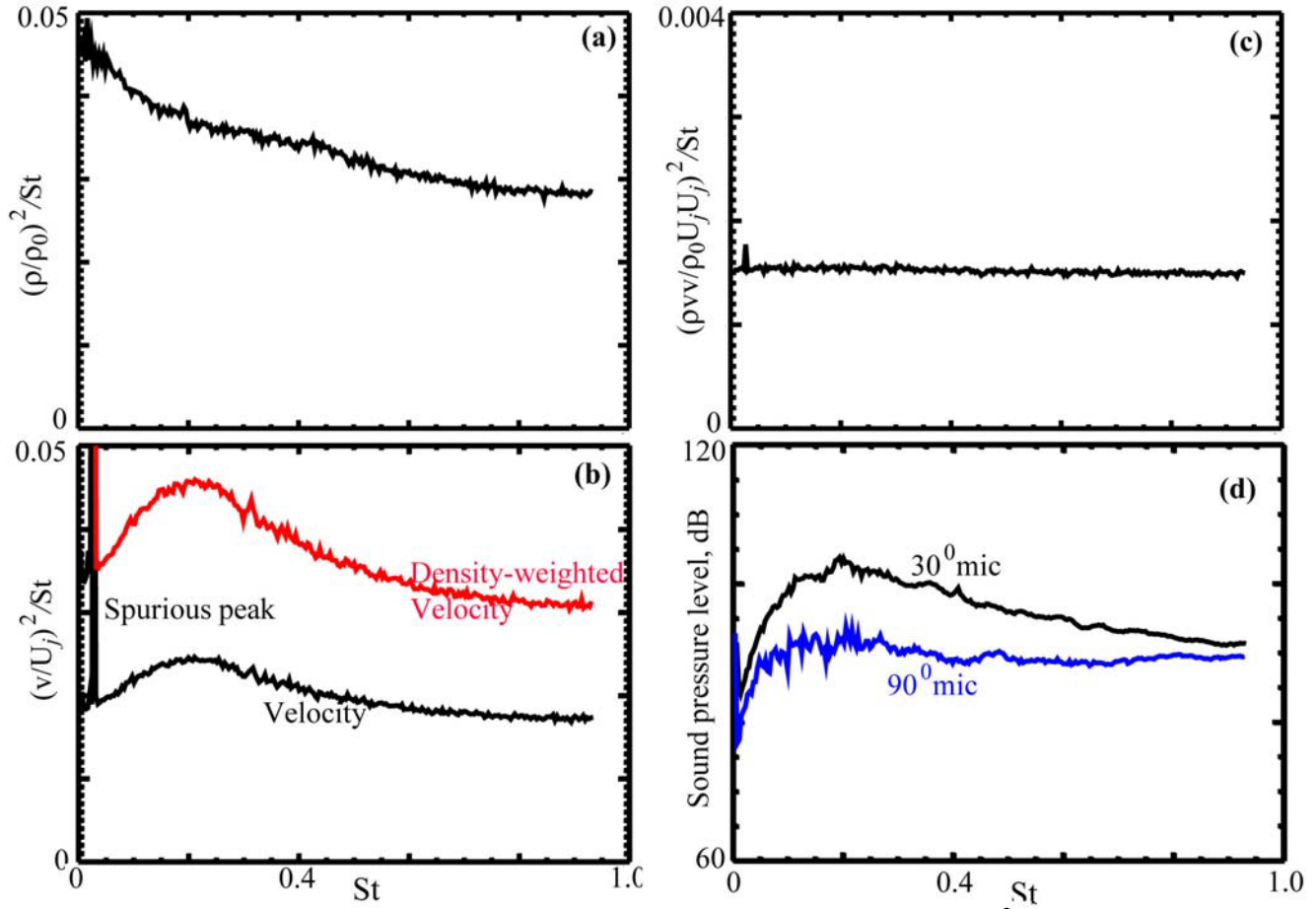
Fig. 8. Spectra of (a) density, (b) radial velocity & (c) density*(radial velocity)² fluctuations in Mach 1.4 jet at centerline & x/D = 10; (d) microphone spectra from indicated azimuthal position and 50D distance from nozzle
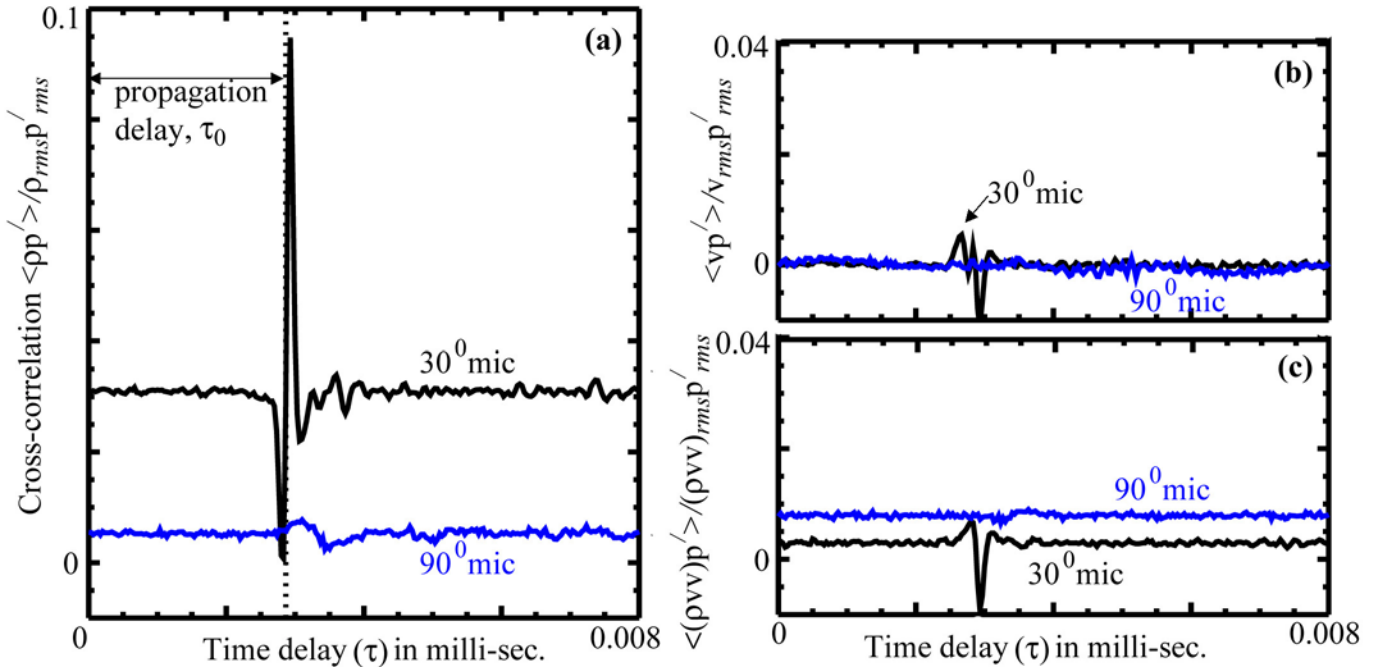
Fig. 9. normalized cross-correlation between microphone pressures and (a) air density ρ (b) radial component of velocity v & (c) ρvv fluctuations measured at x/D=10 and centerline of M=1.4 jet.
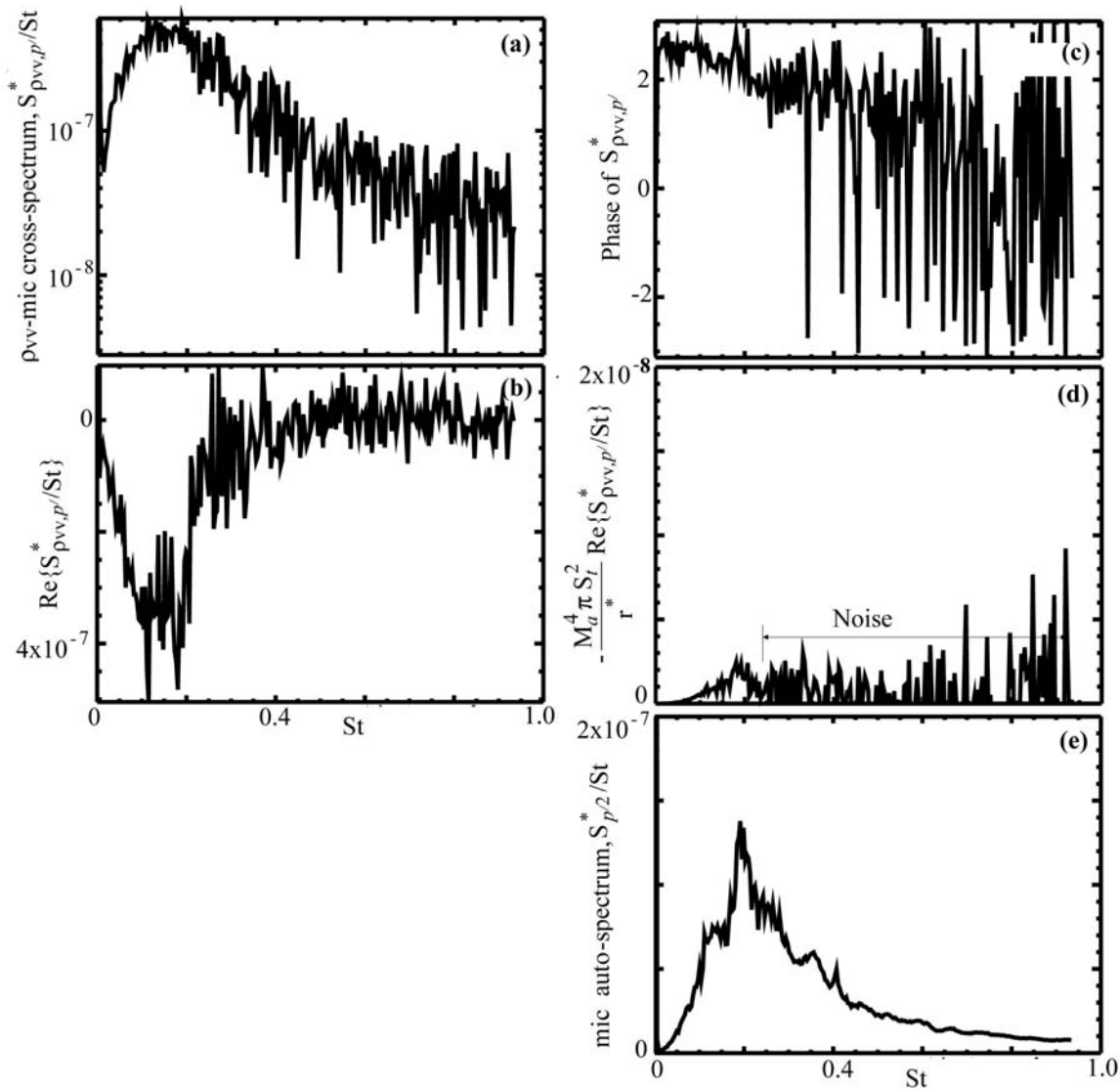
Fig. 10 (a) magnitude of cross-spectrum between 30° microphone and ρvv fluctuations at x/D=10 & centerline of Mach 1.4 jet, (b) real part of cross-spectrum, (c) phase, (d) contribution to sound pressure auto-spectrum (calculated from right hand side of equation 13) and (e) Auto-spectrum of sound pressure fluctuations measured by 30° microphone placed 50 diameters from nozzle exit (left hand side of equation 13)
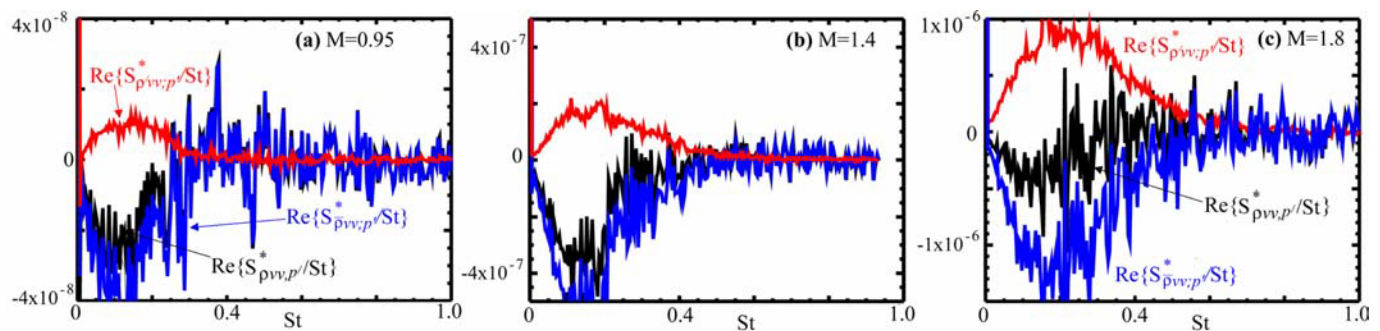
Fig. 11. Real part of cross-spectrum between density*velocity*velocity to 30° microphone obtained by 3 different treatments of density; black curve: when instantaneous density ρ is used; red: fluctuating part ρ′ is used; blue: time average ρ̄ is used. Probe location for (a) x/D=10, centerline, M=0.95, (b) x/D=10, centerline, M=1.4, (c) x/D=14, centerline, M=1.8.
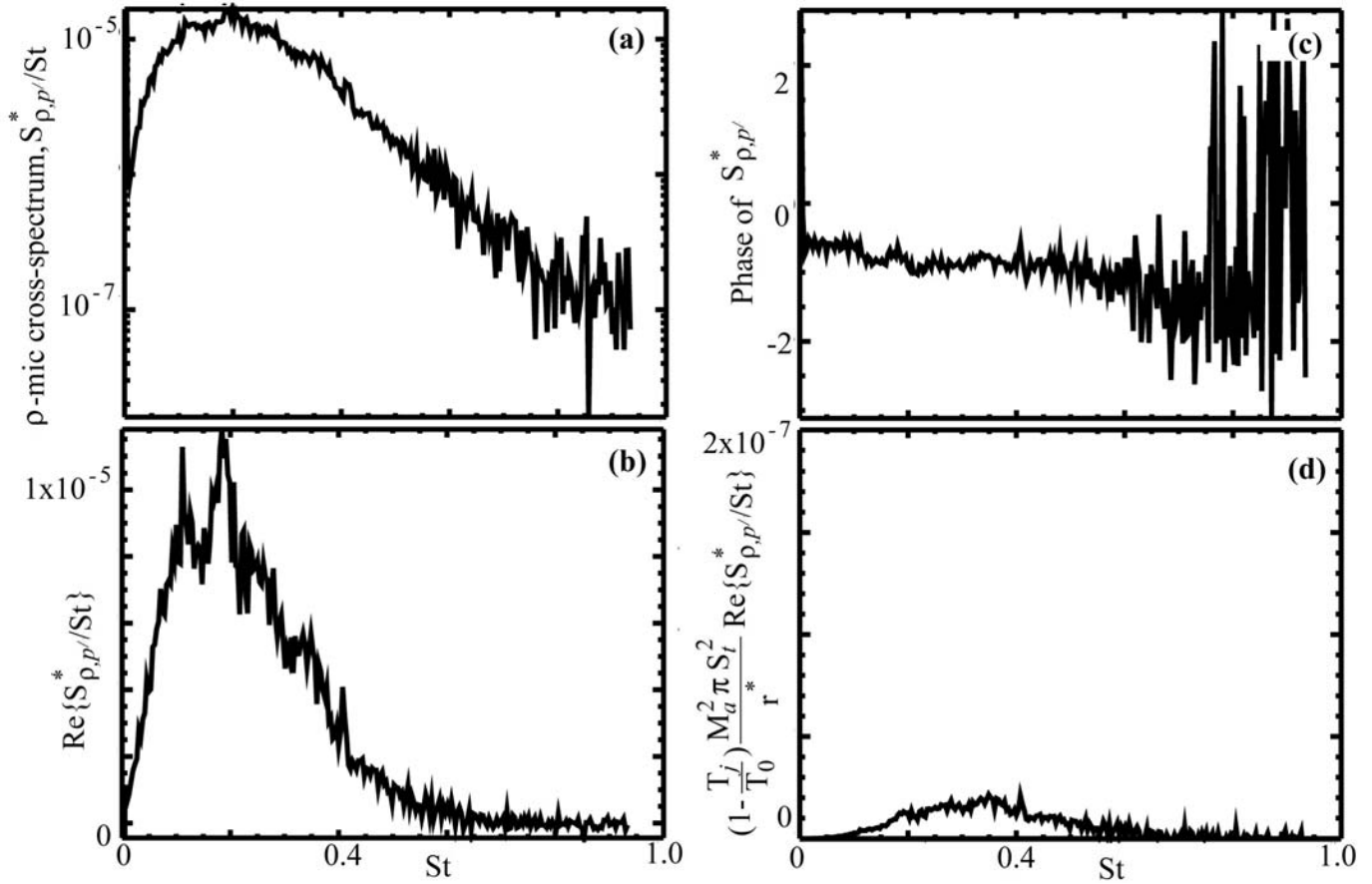
Fig. 12 (a) magnitude of cross-spectrum between 30° microphone signal and density fluctuations from x/D=10 & centerline of Mach 1.4 jet; (b) real part of cross-spectrum, (c) phase and (d) contribution to the sound pressure auto-spectrum (calculated from right hand side of equation 14)
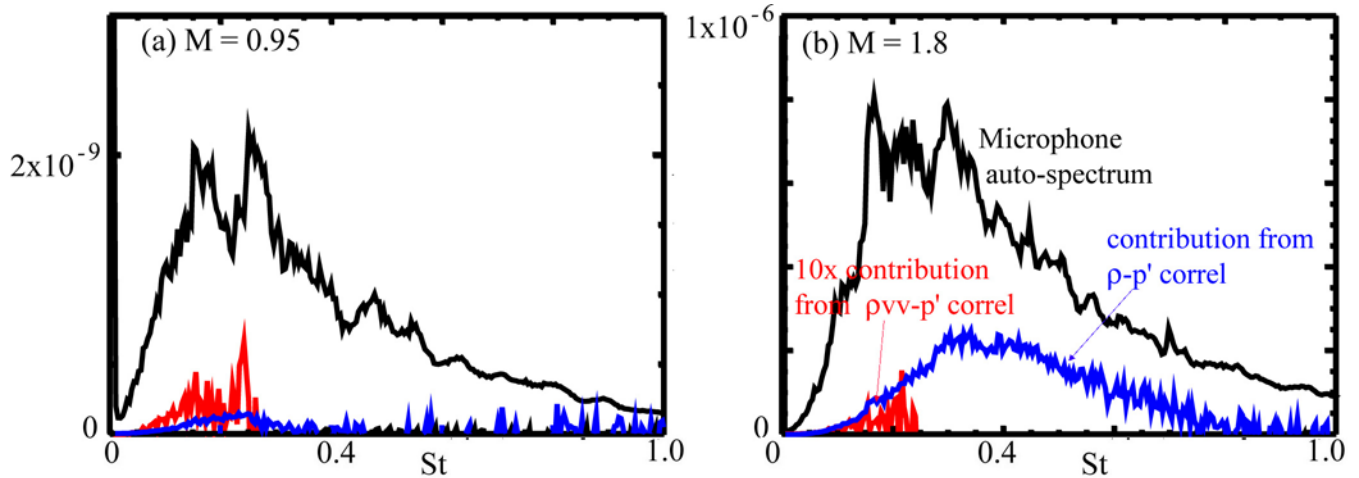
Fig. 13. Relative contribution to the 30°-microphone auto-spectrum from ρvv-p' and ρ-p' correlations measured in the indicated Mach number jets. Laser probe location (a) x/D = 10 & centerline, M=0.95; (b) x/D = 14 & centerline, M = 1.8.
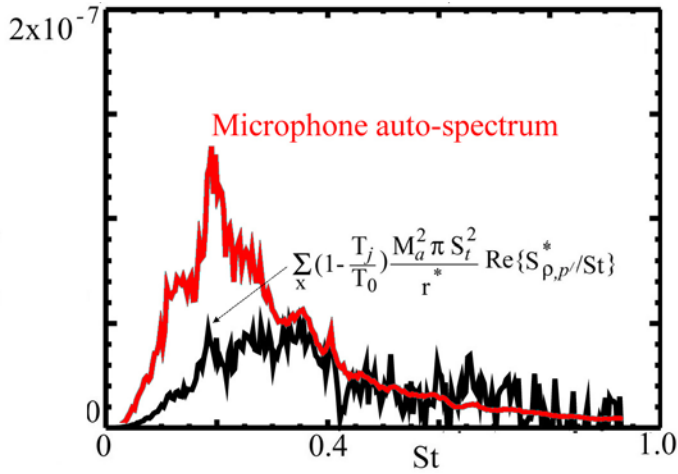
Fig. 14. Auto spectrum of 30° microphone signal and summed up contribution to the noise produced at 50D and 30° to jet axis from ρ-p' cross spectrum measured along centerline and x/D = 2, 4, 6, 8, 10, 12 and 14 of Mach 1.4 jet.
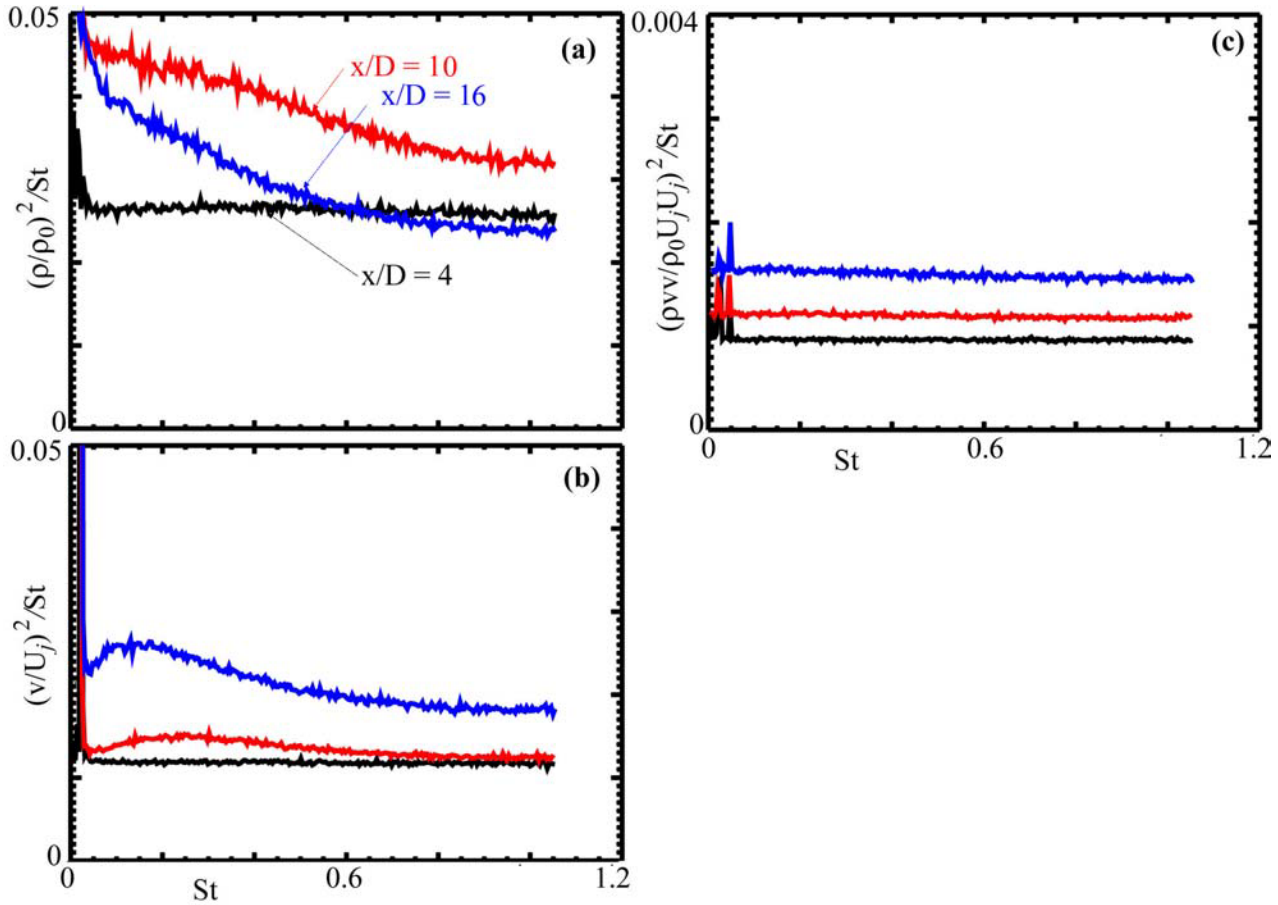
Fig. 15. Spectra of (a) density, (b) radial velocity & (c) density*(radial velocity)^2 fluctuations in Mach 1.8 jet at indicated axial stations along centerline.
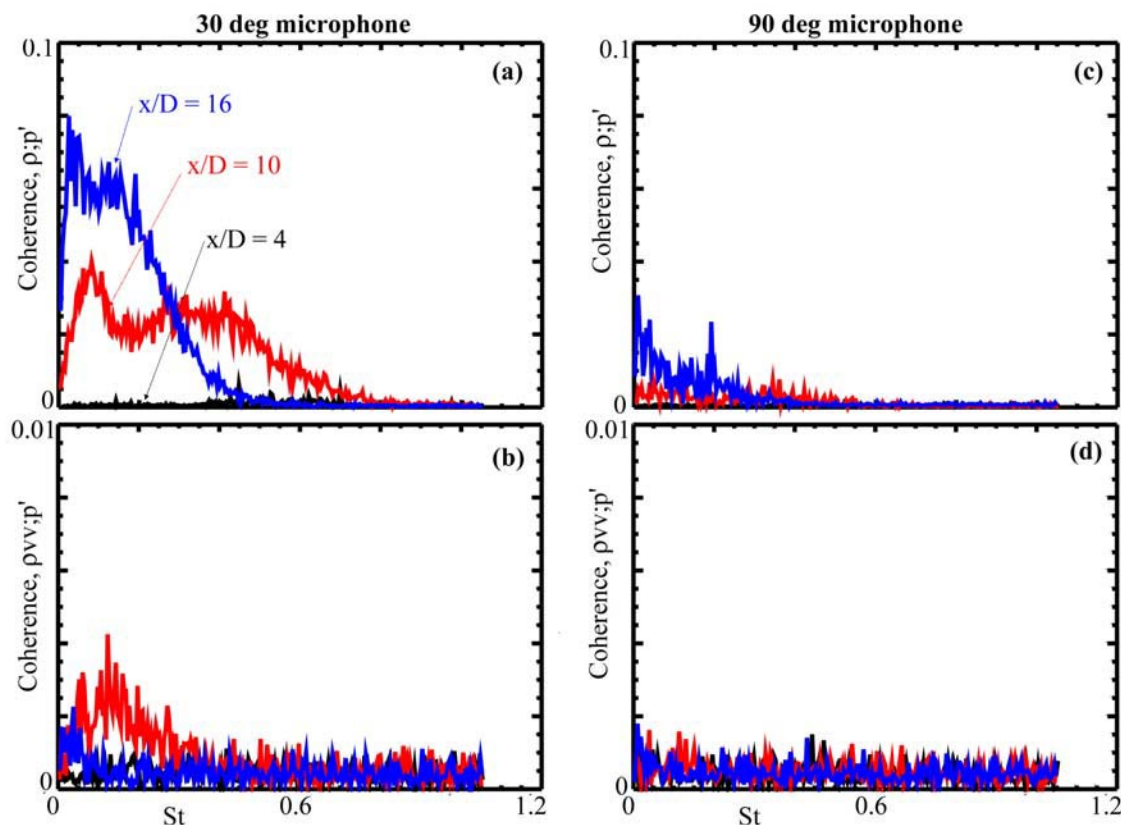
Fg. 16. Coherence functions measured by correlating indicated microphone signals with flow density & density*(radial velocity)^2 fluctuations at indicted axial positions on *centerline of Mach 1.8 jet*; (a) $\Gamma^2_{\rho, 30°}$ (b) $\Gamma^2_{\rho vv, 30°}$, (c) $\Gamma^2_{\rho, 90°}$, (d) $\Gamma^2_{\rho vv, 90°}$.
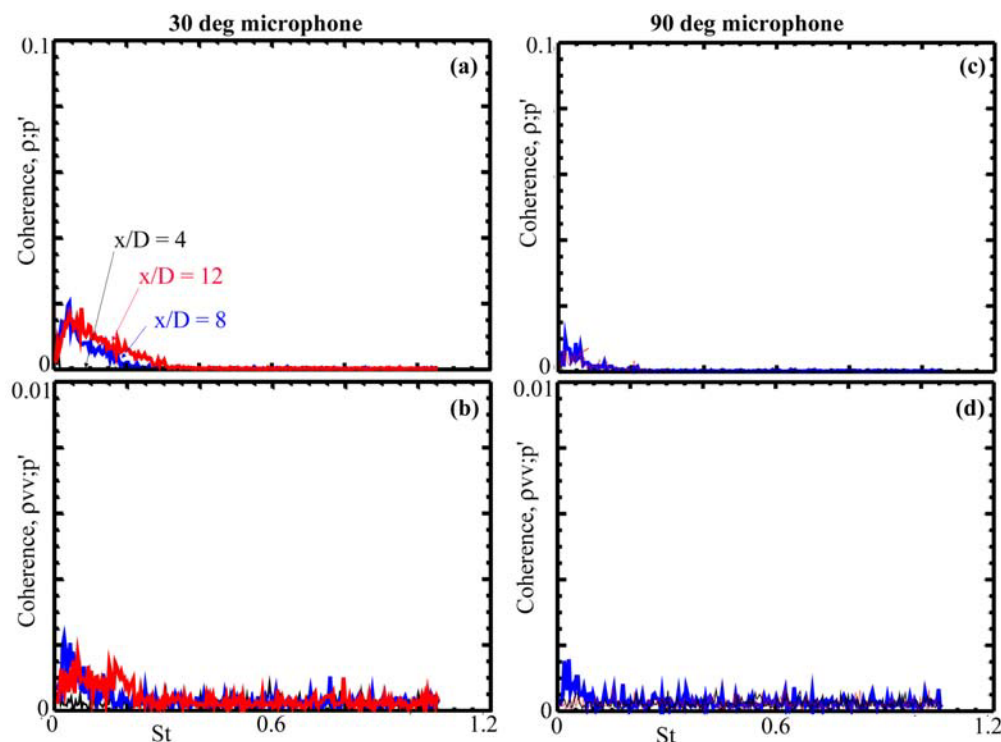
Fig. 17. Coherence functions measured by correlating indicated microphone signals with flow density, radial velocity & density*(radial velocity)^2 fluctuations measured at indicted axial positions on *centerline of Mach 0.95 jet*; (a) $\Gamma^2_{\rho, 30°}$ (b) $\Gamma^2_{\rho vv, 30°}$, (c) $\Gamma^2_{\rho, 90°}$, (d) $\Gamma^2_{\rho vv, 90}$

REPORT DOCUMENTATION PAGE

1. AGENCY USE ONLY (Leave blank)	2. REPORT DATE	3. REPORT TYPE AND DATES COVERED
	September 2002	Technical Memorandum

4. TITLE AND SUBTITLE

Measurement of Correlation Between Flow Density, Velocity, and Density*Velocity^2 With Far Field Noise in High Speed Jets

5. FUNDING NUMBERS

WU–708–90–43–00

6. AUTHOR(S)

Jayanta Panda, Richard G. Seasholtz, and Kristie A. Elam

7. PERFORMING ORGANIZATION NAME(S) AND ADDRESS(ES)

National Aeronautics and Space Administration
John H. Glenn Research Center at Lewis Field
Cleveland, Ohio 44135–3191

8. PERFORMING ORGANIZATION REPORT NUMBER

E–13485

9. SPONSORING/MONITORING AGENCY NAME(S) AND ADDRESS(ES)

National Aeronautics and Space Administration
Washington, DC 20546–0001

10. SPONSORING/MONITORING AGENCY REPORT NUMBER

NASA TM—2002-211791
AIAA–2002–2485

11. SUPPLEMENTARY NOTES

12a. DISTRIBUTION/AVAILABILITY STATEMENT

Unclassified - Unlimited
Subject Category: 45   Distribution: Nonstandard

Available electronically at http://gltrs.grc.nasa.gov

This publication is available from the NASA Center for AeroSpace Information, 301–621–0390.

12b. DISTRIBUTION CODE

13. ABSTRACT (Maximum 200 words)

To locate noise sources in high-speed jets, the sound pressure fluctuations p', measured at far field locations, were correlated with each of radial velocity v, density ρ, and ρv^2 fluctuations measured from various points in jet plumes. The experiments follow the cause-and-effect method of sound source identification, where $\langle \rho v^2 \text{-} p' \rangle$ correlation is related to the first, and $\langle \rho\text{-}p' \rangle$ correlation to the second source terms of Lighthill's equation. Three fully expanded, unheated plumes of Mach number 0.95, 1.4 and 1.8 were studied for this purpose. The velocity and density fluctuations were measured simultaneously using a recently developed, non-intrusive, point measurement technique based on molecular Rayleigh scattering. It was observed that along the jet centerline the density fluctuation spectra S_ρ have different shapes than the radial velocity spectra S_v, while data obtained from the peripheral shear layer show similarity between the two spectra. Density fluctuations in the jet showed significantly higher correlation, than either ρv^2 or v fluctuations. It is found that a single point $\langle \rho\text{-}p' \rangle$ correlation from the peak sound emitting region at the end of the potential core can account for nearly 10% of all noise at 30° to the jet axis. The $\langle \rho v^2\text{-}p' \rangle$ correlation, representing the effectiveness of a longitudinal quadrupole in generating noise 90° to the jet axis, is found to be zero within experimental uncertainty. In contrast ρv^2 fluctuations were better correlated with sound pressure fluctuation at the 30° location. The strongest source of sound is found to lie at the centerline and beyond the end of potential core.

14. SUBJECT TERMS

Rayleigh scattering; Jet aircraft noise

15. NUMBER OF PAGES

27

16. PRICE CODE

17. SECURITY CLASSIFICATION OF REPORT	18. SECURITY CLASSIFICATION OF THIS PAGE	19. SECURITY CLASSIFICATION OF ABSTRACT	20. LIMITATION OF ABSTRACT
Unclassified	Unclassified	Unclassified	